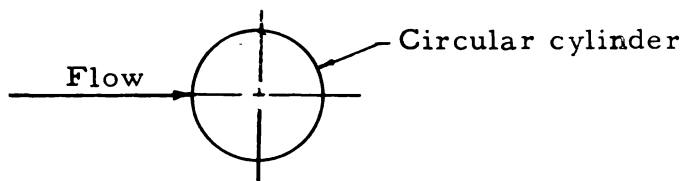


ABSTRACT

THE EFFECT OF FREE STREAM TURBULENCE INTENSITY ON THE BOUNDARY LAYER TRANSITION AROUND A CIRCULAR CYLINDER

by Haribhajan Singh Kocher

The object of this investigation was to study the effect of the free stream turbulence intensity on the transition from laminar to turbulent flow in the boundary layer around a circular cylinder. All the measurements were made in subsonic flow at the Reynolds number, based on the cylinder diameter and free stream velocity, of $1.54 (10)^5$. The relationship of the fluid flow to the circular cylinder is shown below:



Various free stream turbulence intensities were achieved with turbulence generating grids made of circular metallic rods of various diameters. The mesh length was maintained constant as one inch. A traverse mechanism was designed with which it was possible to locate the hot wire anemometer probe filament at any angle from the stagnation point and at any desired distance from the circular cylinder accurately.

The boundary layer transition was investigated by obtaining (a) skin friction intensity distribution around the cylinder, (b) velocity profiles across the boundary layer at various angles including the transition region, (c) fluctuations of the velocity parallel to the cylinder surface at various

angles including the transition region. In the case of skin friction distributions around the cylinder a sharp minimum followed by an increase in the skin friction and a sharp maximum before the skin friction gradually becomes zero have been observed by Fage and Faulkner [8] and Giedt [12]. The sharp maximum and minimum points in the skin friction distribution curves were not observed during the present investigation. Instead, large fluctuations in the skin friction in the transition region were observed. The fluctuations did not represent a scattering of data, because the fluctuations were obtained when the measurements were repeated several times. It is believed that the fluctuations were caused by turbulent spots. The velocity profiles at various stations around the circular cylinder including the transition region were obtained. A part of the results were quite conclusive in establishing transition, while the rest proved unsuccessful. Due to the incapability of these results in establishing the transition region accurately and the impracticability of measuring velocity profiles at intervals of one degree this method was given up in favor of observing the fluctuations in the velocity parallel to the cylinder surface. The fluctuations of velocity parallel to the cylinder surface were recorded by photographing the screen of a cathode ray oscilloscope with a polaroid camera. The elimination of oscillations below 1000 cps with electronic filters made the results extremely clear. This method proved highly successful in defining the transition region. The existence of turbulent spots, and the intermittent nature of the flow in the boundary layer were clearly observed in the transition region.

It was observed that an increase in the free stream turbulence intensity caused the point of origin of the transition region to move away from the stagnation point.

It was also noticed that an increase of free stream turbulence intensity produced an increase of steepness in the velocity profiles in the outer

region of the boundary layer around a circular cylinder, which means that further deviation of the velocity profiles in the outer part of the boundary layer from the Blasius profiles takes place as the free stream level of turbulence increases. The most probable reason considered for this phenomenon was the diffusion of turbulence in the outer part of the boundary layer.

THE EFFECT OF FREE STREAM TURBULENCE INTENSITY ON THE
BOUNDARY LAYER TRANSITION AROUND
A CIRCULAR CYLINDER

By

Haribhajan Singh Kocher

A THESIS

Submitted to
Michigan State University
in partial fulfillment of the requirements
for the degree of

DOCTOR OF PHILOSOPHY

Department of Applied Mechanics

1962

g29073
6/24/64

ACKNOWLEDGMENTS

It is a pleasure for the author to express his sincere gratitude to Professor Charles O. Harris for his able supervision, unfailing interest and constant encouragement throughout the project.

Thanks are also due to Dr. Clement A. Tatro for his immense help in instrumentation and as a major professor, and the other members of his guidance committee: Dr. Terry Triffet, Dr. C. P. Wells, and Dr. J. E. Lay.

Finally, to Surjit S. Dulai, Kartar S. Kocher, and Albert Brownell, the author is thankful for their help and friendship.

TABLE OF CONTENTS

CHAPTER	Page
I. TRANSITION AND ITS INVESTIGATION	1
Introduction to Transition from Laminar to Turbulent Flow	1
Various Techniques of Investigating Transition . . .	3
II. THE THEORIES AND MECHANICS OF TRANSITION . . .	9
III. DESCRIPTION OF APPARATUS AND PROCEDURES . . .	12
The Wind Tunnel and the Cylinder	12
The Traverse Mechanism	15
The Turbulence Grids and Intensity Measurement . .	24
Determination of Velocity Profiles	26
Determination of Pressure Coefficient Distribution .	38
IV. PRESENTATION AND DISCUSSION OF RESULTS	40
Coefficient of Pressure Distribution	40
Intensity of Skin Friction Distribution	40
Velocity Profiles	42
Observation of Turbulent Spots	57
V. CONCLUSIONS	63
SUGGESTED PROBLEMS	65
BIBLIOGRAPHY	67

LIST OF FIGURES

FIGURE	Page
1. Rising smoke column from a cigarette.	2
2. A schematic representation of the laminar flow stability	10
3. Oscillograms representing the extraneous waves in the testing section of the wind tunnel, and a typical square wave for calibration.	13
4. Frequency of the extraneous wave for various fan speeds.	14
5. Measurement of velocity pressure in the testing section with and without cylinder with the pitot tube at the same location.	16
6. A typical velocity distribution in the testing section of the wind tunnel.	18
7. Measurement of turbulence intensity at the central plane normal to the flow in the testing section.	19
8. Elevation view of the traverse mechanism.	21
9. Plan view of the traverse mechanism.	22
10A. Various instruments (excluding the hot wire anemometer probe) used in the present investigation.	25
10B. A typical section of the turbulence grid	25
11. Calibration curve (voltage vs. frequency) for the voltage to frequency converter.	27
12. Calibration curve (voltage vs. frequency) for the voltage to frequency converter	28

LIST OF FIGURES - Continued

FIGURE	Page
13. Turbulence intensity of free stream three inches ahead of the stagnation point for various turbulence generating grids.	30
14. A typical calibration curve for the hot wire anemometer probe filaments used during the present investigation.	31
15. Velocity profile across the boundary layer for $\Theta = 30^\circ$	34
16. Velocity profile across the boundary layer at $\Theta = 40^\circ$.	35
17. Velocity profile across the boundary layer at $\Theta = 60^\circ$.	36
18. Velocity profiles across the boundary layer at various turbulence intensities at $\Theta = 60^\circ$	37
19. Coefficient of pressure distributions around the circular cylinder for various turbulence intensities and Reynolds number of $1.54(10)^5$	41
20. Skin Friction distributions around a circular cylinder for turbulence intensity of 0.82%.	43
21. Skin friction distribution around the circular cylinder for turbulence intensity of 2.09%.	44
22. Skin friction distribution around the circular cylinder for turbulence intensity of 2.80%.	45
23. Skin friction distribution around the circular cylinder for turbulence intensity of 3.62%.	46
24. Skin friction distribution around the circular cylinder for turbulence intensity of 4.40%.	47
25A. Velocity Profiles in the boundary layer around the circular cylinder for turbulence intensity of 0.82%.	49
25B. Velocity Profiles in the boundary layer around the circular cylinder for turbulence intensity of 0.82%.	50

LIST OF FIGURES - Continued

FIGURE	Page
26A. Velocity Profiles in the boundary layer around the circular cylinder for turbulence intensity of 2.09%.	51
26B. Velocity Profiles in the boundary layer around the circular cylinder for turbulence intensity of 2.09%.	52
27A. Velocity Profiles in the boundary layer around the circular cylinder for turbulence intensity of 2.80%.	53
27B. Velocity Profiles in the boundary layer around the circular cylinder for turbulence intensity of 2.80%.	54
28A. Velocity Profiles in the boundary layer around the circular cylinder for turbulence intensity of 3.62%.	55
28B. Velocity Profiles in the boundary layer around the circular cylinder for turbulence intensity of 3.62%.	56
29. Velocity fluctuation, u , in the boundary layer around a circular cylinder for turbulence intensities of 0.82% and 2.09%.	59
30. Velocity fluctuation, u , in the boundary layer around a circular cylinder for turbulence intensities of 2.80%, and 3.62%.	60
31. Velocity fluctuation, u , in the boundary layer around a circular cylinder for turbulence intensities of 3.62%, and 4.47%.	61
32. Transition Region around a circular cylinder for various turbulence intensities.	62

Symbol	Notations	Units
D	Diameter of the cylinder	feet
$\frac{C_f}{2}$	Intensity of skin friction	--
Cp	Coefficient of pressure	--
H	Heat transferred from the hot wire anemometer probe filament per unit time	watts
Hp	Heat loss from the hot wire probe filament to a flat plate	watts
I	Current passing through the hot wire probe filament	amperes
k	Thermal conductivity	btu ft ⁻¹ sec ⁻¹ ok ⁻¹
ℓ	Length of the filament	feet
p	Pressure	lb _f ft ⁻²
p'	Excess of local static pressure p ₀ +p' over the free stream static pressure	lb _f ft ⁻²
Pr	Prandtl number ($\frac{C_p \mu}{k}$)	--
q ₀	Heat flux	btu ft ⁻² sec ⁻¹
Re	Reynolds number ($\frac{U_\infty D}{\nu}$)	--
Rw	Electrical resistance of the hot wire probe filament	ohms
Tw	Wall temperature	^o K
T	Free stream temperature	^o K
U _(x)	Local velocity of the flow just outside the boundary layer	ft. sec ⁻¹
U _(∞)	Free stream velocity	ft. sec ⁻¹
u	Deviation of U about \bar{U}	ft. sec ⁻¹
u'	Root mean square of u	ft. sec ⁻¹
v	Deviation of V about \bar{V}	ft. sec ⁻¹
x	Coordinate parallel to the cylinder surface	ft.
y	Coordinate perpendicular to the cylinder surface	ft.

Continued

Symbol	Notations	Units
δ	Boundary layer thickness	ft.
δ^*	Displacement thickness	ft.
μ	Viscosity	$\text{lb}_f \text{ sec ft}^{-2}$
ν	Kinematic viscosity	$\text{ft}^2 \text{ sec}^{-1}$
δ	Density	$\text{lb}_m \text{ ft}^{-3}$
τ_o	Skin friction	$\text{lb}_f \text{ ft}^{-2}$
θ	Angle measured from the stagnation point	degrees

CHAPTER I

TRANSITION AND ITS INVESTIGATION

Introduction to Transition from Laminar to Turbulent Flow

Laminar fluid flow is characterized by a well-ordered movement of particles. The individual particles form layers which travel in regular paths parallel to the solid boundaries, and there is no velocity component normal to the solid boundary. In turbulent flow this orderliness breaks down, and there is considerable mixing of the fluid during flow. A particle of fluid has an average velocity parallel to the solid boundary, but its motion is chaotic, and it has velocity components both parallel and normal to solid boundary at all times. Everybody has observed transition in the case of a rising smoke column from a cigarette as shown in Figure 1. In 1882, Osborne Reynolds [21] observed that under certain circumstances transition from laminar to turbulent flow took place in circular tubes. Since then, transition has been observed in various types of flow, e. g., free flow, boundary layer flow, etc. The conditions known so far to affect the occurrence of transition have been found to be as follows:

- (1) Surface cooling or heating (surface is that of solid boundary along which the fluid flow occurs).
- (2) Surface curvature.
- (3) Surface roughness.
- (4) Surface pressure gradient.
- (5) Surface temperature gradient.
- (6) Suction and injection through surface.
- (7) Reynolds number of the free stream.



FIGURE 1. Rising smoke column from a cigarette.

- (8) Intensity of turbulence in the free stream.
- (9) Scale of turbulence in the free stream.
- (10) Sound propagation and vibration through free stream and solid boundary.
- (11) Magnetic field intensity in the free stream.
- (12) Mach number of free stream.
- (13) Interaction of shock wave with boundary layer.
- (14) Nose shape.

A bibliography on most of the above factors is given in reference [1]. Kuethe and Schetzer [17] also discuss this subject in their textbook.

Transition plays an extremely important role in the diverse fields of engineering. Transition can prove beneficial by delaying separation of flow or promoting rapid diffusion of momentum, matter and heat. It can also prove detrimental by increasing skin friction and rates of heat-transfer as in ultra high supersonic flight of airplanes and missiles. Consequently, an understanding of this widely observed flow phenomenon is of great practical significance to aeronautical development.

Since the problem of transition is extremely difficult to handle theoretically, it is, therefore, very important to consider the various techniques and criteria available for investigating transition experimentally. Their discussion follows.

Various Techniques of Investigating Transition

1. Turbulent Shearing Stresses

It is generally recognized that the fundamental difference between the fluctuations in turbulent and laminar parts of the boundary layer is one of correlation between the velocity fluctuations, u , parallel to a solid boundary and v , normal to it. If the instantaneous values of u - and v -fluctuations are denoted by u_i and v_i respectively, the essential difference

may be expressed in terms of the value of $\overline{u_1 v_1}$, where the bar denotes the the average value. The turbulent shearing stress is given by $\overline{u_1 v_1}$. A turbulent shearing stress must be absent in a laminar boundary layer and $\overline{u_1 v_1}$ must be zero. By definition, a turbulent or partly turbulent layer is one in which a turbulent shearing stress exists, that is, $\overline{u_1 v_1}$ has a value other than zero. The value of $\overline{u_1 v_1}$ therefore furnishes the best criterion to establish whether the boundary layer is laminar or turbulent. $\overline{u_1 v_1}$ can be measured with the help of a two channel hot wire anemometer. For theory and instructions regarding the measurement of $\overline{u_1 v_1}$ the reader is referred to [10] and [13].

2. Surface Temperature

It has been observed that there is a marked increase in the temperature recovery factor, i. e. the ratio of the frictional temperature increase of the plate ($T_{ad} - T_{\infty}$), to that due to adiabatic compression, in the transition region, thus measurements of equilibrium temperature of an insulated surface provides a practical means for determining the transition region. For flows of short duration, the surface will not reach an equilibrium temperature, but since the skin friction is considerably greater in the turbulent region than in the laminar, the rate of heat transfer to the surface will be much greater in the transition region. Reference [15] provides more information on this subject.

3. Density Gradient

Magnified Schlieren photographs sensitive to the density gradients normal to surface provide an accurate means of locating transition. For information regarding the experimental set up and theory refer to [4].

4. Sublimation

This method utilizes a coating of a volatile substance on the surface; the rate of sublimation depends upon whether the boundary layer is

laminar or turbulent. The greater velocity gradient at the surface in the turbulent layer causes a higher rate of sublimation than if the layer is laminar. Consequently, behind the transition region the surface will clean more rapidly than ahead, and the line of demarcation marks the transition point. Refer to [20] for further information.

5. Presence of Turbulent Spots

Turbulent spots have been observed to be present in the transition region [24]. These high frequency spots can be recorded with the help of a hot wire anemometer in the form of oscillograms. These spots have also been detected with the help of a medical stethoscope, which is applied to short tubes leading from total head tubes in the boundary layer. A steady noise is heard when the total head tube is in the turbulent boundary layer.

6. Boundary Layer Thickness

It is well-known that boundary layer thickness increases remarkably as transition begins, and the thickness of the turbulent part of the boundary layer is considerably larger than that of the laminar part. The boundary layer thickness can be found experimentally with the help of hot wire anemometer or small total head tubes.

7. Mean Velocity Profiles

Mean velocity profiles can be employed to determine whether flow at a given station of solid boundary is laminar or turbulent. For laminar flow the velocity profiles resemble the Blasius profiles closely, and in the transition region change progressively till they acquire the form of a turbulent profile. Schubauer and Klebanoff [24] have used this method quite successfully.

8. Skin Friction

Transition on a flat plate involves a large change in the resistance to flow, or skin friction. In laminar flow the skin friction is proportional to the 1.5 power of the velocity, whereas in turbulent flow the power increases to 1.85, as shown a long time ago by Froude [10]. Fage and Faulkner [8] and Geidt [12] determined the skin friction intensity distribution around a circular cylinder by using small surface tubes. They obtained a minimum for those cases in which transition occurred before separation. They regarded the minimum in their curves as the beginning of the transition region. For the laminar part of the boundary layer, their skin friction distribution intensity curves resemble the Blasius curves closely in form, but not too closely in magnitude.

For continuum flow with no slip at the solid surface the skin friction, τ_0 , at any point on a solid surface in a flowing gas is given by

$$\tau_0 = \left(\mu \frac{\partial U}{\partial y} \right)_{y=0} \quad (1)$$

It is known that for the flow of gases at temperatures and pressures at which the mean free paths of the gas molecules are small compared with the physical dimensions of the system, the slip at the solid boundary is negligible.

The above expression for skin friction is valid for laminar, and, because of the existence of a laminar sub-layer, also for turbulent boundary layers. In general, experimental attempts at measurements of the skin friction may be classified into two main types:

1. Those which endeavor to determine the components of the right hand side of the equation (1).
2. Those which rely on a bulk measurement of the skin friction, or some other quantities related to it.

(a) Skin friction by velocity profile method. In this type of measurement, the physical quantities to be measured are the viscosity μ and the velocity U in the boundary layer. Kinetic theory and experiment indicate the viscosity coefficient to be a function of the absolute temperature T alone. Thus a local measurement of the wall temperature with a sensitive thermocouple is sufficient to define $(\mu)_{y=0}$. The measurement of the velocity as a function of the normal coordinate y can be made with any of the following instruments:

- (1) Pitot (or total head) tube
- (2) Stanton tube
- (3) Hot wire anemometer
- (4) Interferometer

(b) Skin friction by direct method. The second type of skin friction measurement, relying on a bulk measurement, may be performed in principle in two ways:

- (1) By a heat transfer method.
- (2) By a direct force determination.

(c) Skin friction by heat transfer measurement. This method depends on Reynolds analogy between the transfer of momentum and heat. If q_0 is the heat flow per unit time for a unit area of the surface and k is the heat conductivity of the fluid, then

$$q_0 = k \left(\frac{\partial T}{\partial y} \right)_{y=0} \quad (2)$$

where T is the local temperature. The analogy with the expression (1) for the skin friction is at once apparent. For the case of two dimensional flow with Prandtl number $(Pr) \frac{C_p \mu}{k} = 1$ the temperature T is a parabolic function of the velocity U alone. In such a case the heat flow q_0 and the wall shearing stress τ_0 may be explicitly related by an expression [22] of

the form:

$$\left(\frac{q_0}{\tau_0}\right)_x = \frac{1}{U} \left(-\frac{k}{\mu}\right)_{y=0} (T_w - T_\infty) \quad (3)$$

In the above relation assumptions of laminar flow and the equal orders of magnitude for the momentum and thermal boundary layers and incompressibility are evident. For the case when $Pr = 1$, and the flow is turbulent and compressible, then a similar expression may be derived [14]. It is easily seen that estimates of skin friction can be made through measurements of q_0 and the related quantities.

(d) Direct force measurement. In principle the method of direct force is very simple. The frictional force is allowed to move a small element of the surface in the direction of the flow, and against some restoring force. This movement is calibrated to indicate the magnitude of the force. This method was used by early investigators like Froude [11] in determining the fluid resistance of bodies in water. A more recent application is that of Schultz-Grunow [26].

An excellent discussion on the theory, advantages and disadvantages of the various methods given above for skin friction measurement has been presented by Dhawan in reference [3].

CHAPTER II

THE THEORIES AND MECHANICS OF TRANSITION

To explain transition Schlichting, Tollmien and others [19,22] undertook a study of the stability of laminar flow. The fundamental assumption of their study was that small periodic disturbances are assumed to be present at all points in the laminar flow. Their mathematical treatment revealed that instability may occur if a particular value of the Reynolds number $\left(\frac{U_{\infty} \delta^*}{\nu}\right)$ is exceeded. It was further found that for every Reynolds number exceeding this critical value there are two neutral disturbances which are neither amplified nor attenuated. For any intermediate value of wave length (or corresponding frequency) the disturbances are amplified. A schematic diagram is presented in Figure 2. Here, $(Re)_{cr}$ corresponds to the minimum critical Reynolds number, and for any Reynolds number $(Re)_1$, there are two neutral disturbances of frequencies f_1 and f_2 .

In 1936, G. I. Taylor [27] presented a theory which attributed transition to the presence of free stream turbulence. He further assumed that transition due to turbulence resulted from momentary separation of the boundary layer.

The basic difference between these two theories is that the former looks for instability resulting from some inherent characteristic of the laminar flow, whereas the latter requires an external disturbance.

Around 1940, Schubauer and Skramstad [25] reported experimental verification of the Tollmien - Schlichting theory for turbulence intensity less than 0.03%. The current ideas, though by no means universally accepted, are to assume the Tollmien - Schlichting theory valid for

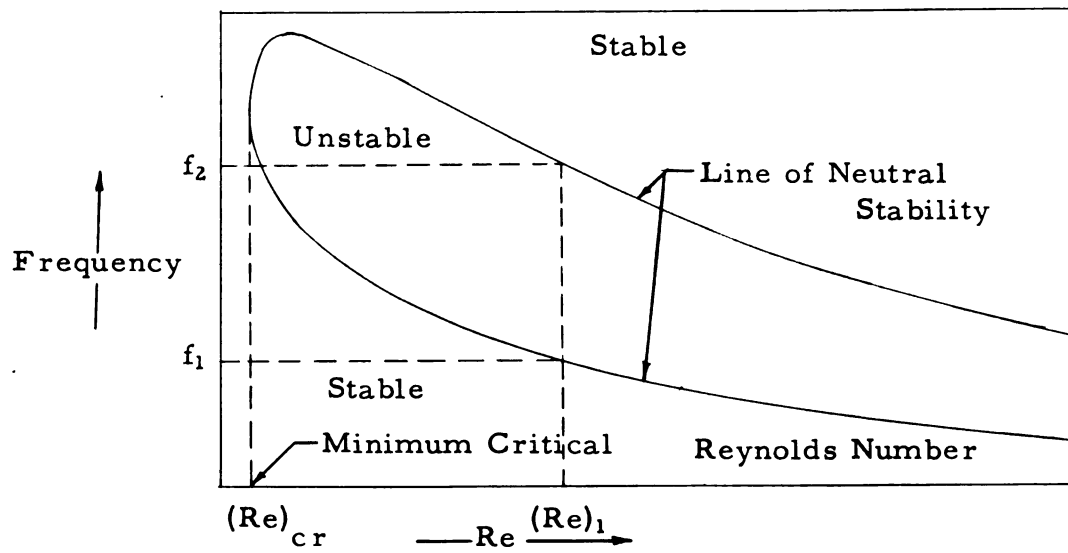


Figure 2. A schematic representation of the laminar flow stability.

intensities of turbulence up to 0.02% and to use Taylor theory for greater values of turbulence intensity.

There is good agreement on the physical model or mechanism of the development of turbulence once it has started. This is solely due to experimental observations, and at present there is no mathematical theory of the transition process.

It has been observed that turbulent spots consisting of small volumes of fluid with turbulent characteristics originate at some points in the flow. The points of origin, in general, are not stationary, but move back and forth slightly. The spots move downstream with the rest of the fluid. As the spots move downstream they grow, and finally break up into smaller spots, causing fully turbulent flow. The appearance, growth and some other very interesting features of these spots have been studied by Emmons [7] and Schubauer and Klebanoff[24]. Still considerable scope exists in the study of these spots.

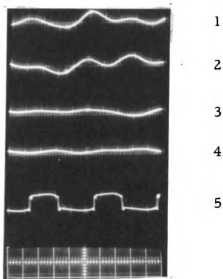
CHAPTER III

DESCRIPTION OF APPARATUS AND PROCEDURES

The Wind Tunnel and the Cylinder

All measurements were made in a wind tunnel of open circuit type. The overall length of the tunnel was 14'-10". The entrance section was rectangular (4 ft. high x 2 ft. wide internally), and the exit was circular (2 ft. in diameter). The testing section was made of transparent lucite. It was rectangular (2 ft. wide x 1 ft. high) normal to the flow direction, and 1 ft. long along the flow.

The tunnel was operated by two heavy duty one horse power motors. Each of these motors drove, through belts, a six blade Aerovent fan of two ft. diameter. The two motor and fan assemblies were connected in series. Both the fans were of suction type, therefore, the whole driving assembly was connected to the tunnel at its exit. It was observed that a certain amount of fan tip noise was propagated through the testing section. Each fan was rated at approximately 72-79 decibels at 1750 rpm, approximately the speed used for the present investigation. Furthermore, a low frequency extraneous wave was observed, as shown in Figure 3. The frequency of this wave depended upon the fan speed, as shown in Figure 4. A considerable effort was made to eliminate this wave. Cork and rubber pads were inserted between the tunnel and the ground. Also, the tunnel and the driving assembly were connected through a rubber buffer. This did not eliminate the wave, however. Consequently it was decided to use an electronic filter to eliminate all signals of frequencies below 25 cps. This did not affect the turbulence signal, because it was negligible below 25 cps, as shown in oscillograms 1 to 4 in Figure 3.



Traces 1 and 2 : Extraneous wave for $U_{\infty}=50$ ft/sec at 0.05 volt/cm and 12 milli sec./cm.

Traces 3 and 4 : Same as above except $U_{\infty}=40$ ft/sec.

Trace 5 : A typical square wave used during the present investigation.

FIGURE 3

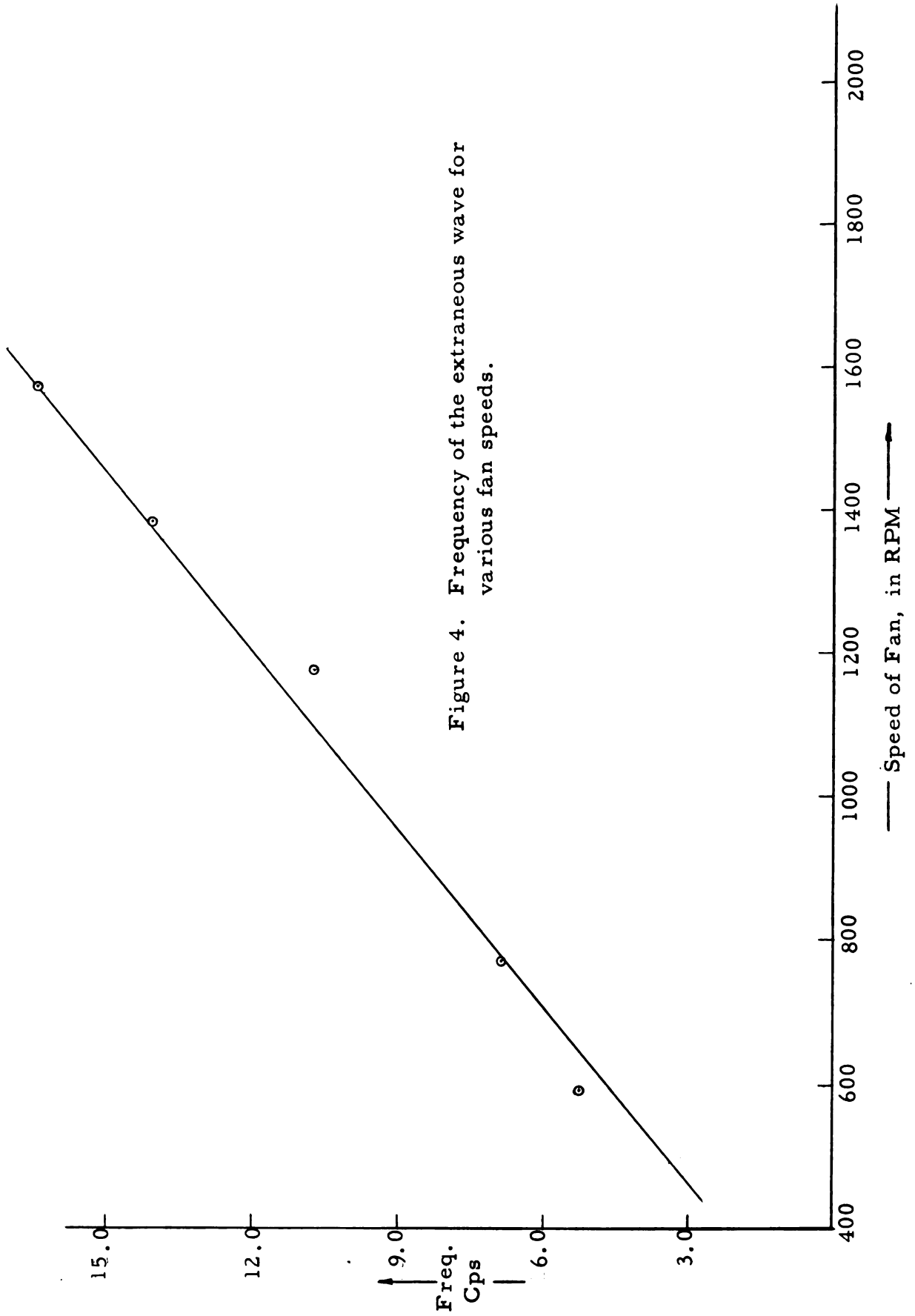


Figure 4. Frequency of the extraneous wave for various fan speeds.

The flow velocities in the testing section were obtained with a pitot tube and Ellison inclined tube manometer using a petroleum oil of 0.834 specific gravity. Since the presence of the cylinder in the testing section affected the velocity distribution considerably, a calibration curve, as shown in Figure 5, was obtained for velocities in the testing section with and without the cylinder for the same location of the pitot tube. The maximum free stream velocity that could be obtained in the testing section was 50 ft. sec⁻¹. The velocity in the testing section was regulated by varying the currents supplied to the motors through variacs.

A commercial test cylinder, six inches in diameter, and twelve inches long with polished brass surface was used for the present investigation. It had static pressure orifices located for 360° at intervals of 10°.

A typical velocity distribution, and turbulence intensity at Reynolds number of 1.54(10)⁵ in the testing section are represented in Figures 6 and 7, respectively.

The Traverse Mechanism

The traverse mechanism is a device which holds the hot wire anemometer probe tightly, and enables to set the hot wire probe filament at any desired location. In this connection it may be mentioned here that the hot wire anemometer is a precision instrument used in measuring average velocities, velocity fluctuations, turbulence intensities and velocity correlations. To enable the determination of velocity and turbulence intensity profiles in the boundary layer, it was decided that this mechanism should fulfill the following two requirements.

- (1) It should be possible to locate the hot wire anemometer profile filament as close as 0.003 inch from the surface of the cylinder, and move it a distance of 0.0005" at a time.

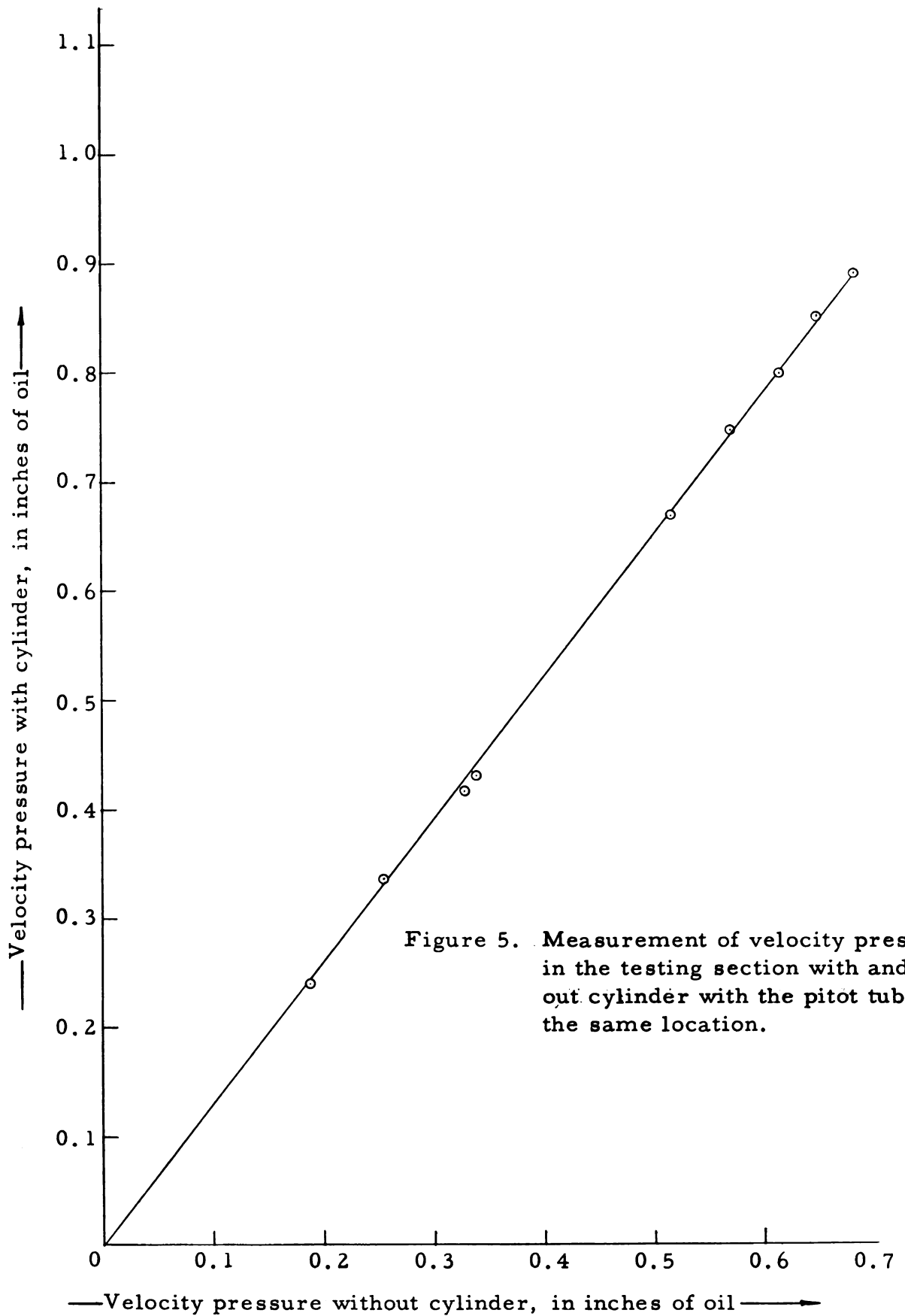
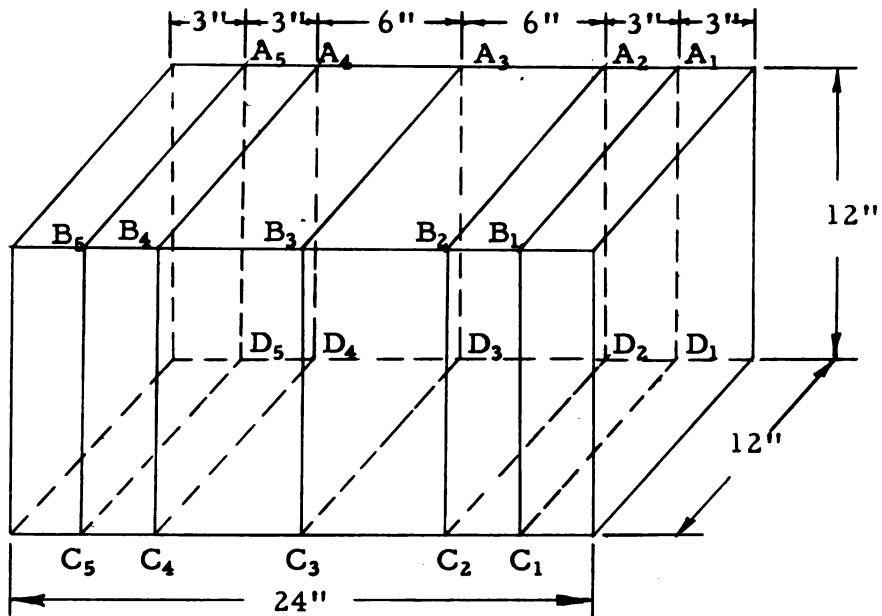


Figure 5. Measurement of velocity pressure in the testing section with and without cylinder with the pitot tube at the same location.

Graph 1. Velocity at various stations in the testing section of the wind tunnel.

Station Number	Velocity (ft./sec.)	Station Number	Velocity (ft./sec.)
1	29.85	31	26.70
2	26.55	32	26.88
3	27.25	33	26.35
4	26.55	34	26.70
5	26.20	35	27.75
6	26.40	36	27.25
7	26.42	37	26.55
8	26.42	38	26.90
9	26.18	39	27.25
10	26.55	40	26.55
11	26.70	41	26.20
12	26.55	42	26.70
13	26.65	43	26.70
14	27.25	44	26.88
15	27.75	45	26.48
16	26.55	46	26.70
17	26.55	47	27.18
18	26.55	48	27.12
19	26.55	49	27.25
20	26.55	50	27.25
21	26.18	51	26.55
22	26.55	52	26.55
23	26.70	53	26.55
24	26.70	54	26.55
25	26.55	55	26.48
26	26.90	56	25.85
27	27.25	57	26.48
28	26.70	58	26.90
29	26.20	59	27.18
30	26.62	60	26.90



Testing Section of the Wind Tunnel

Flow

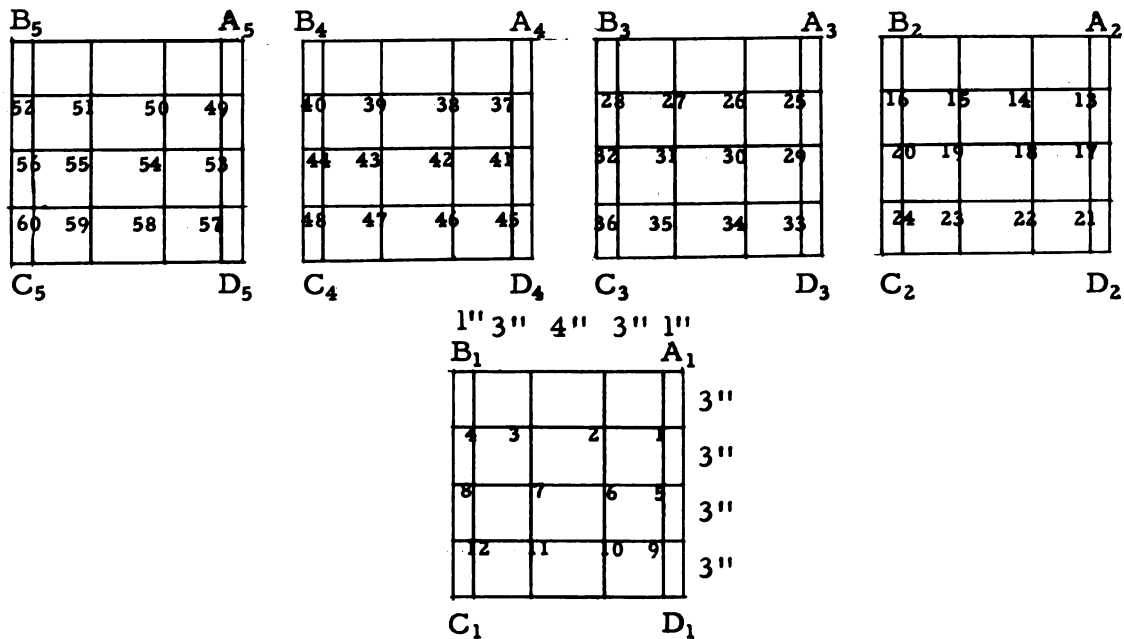
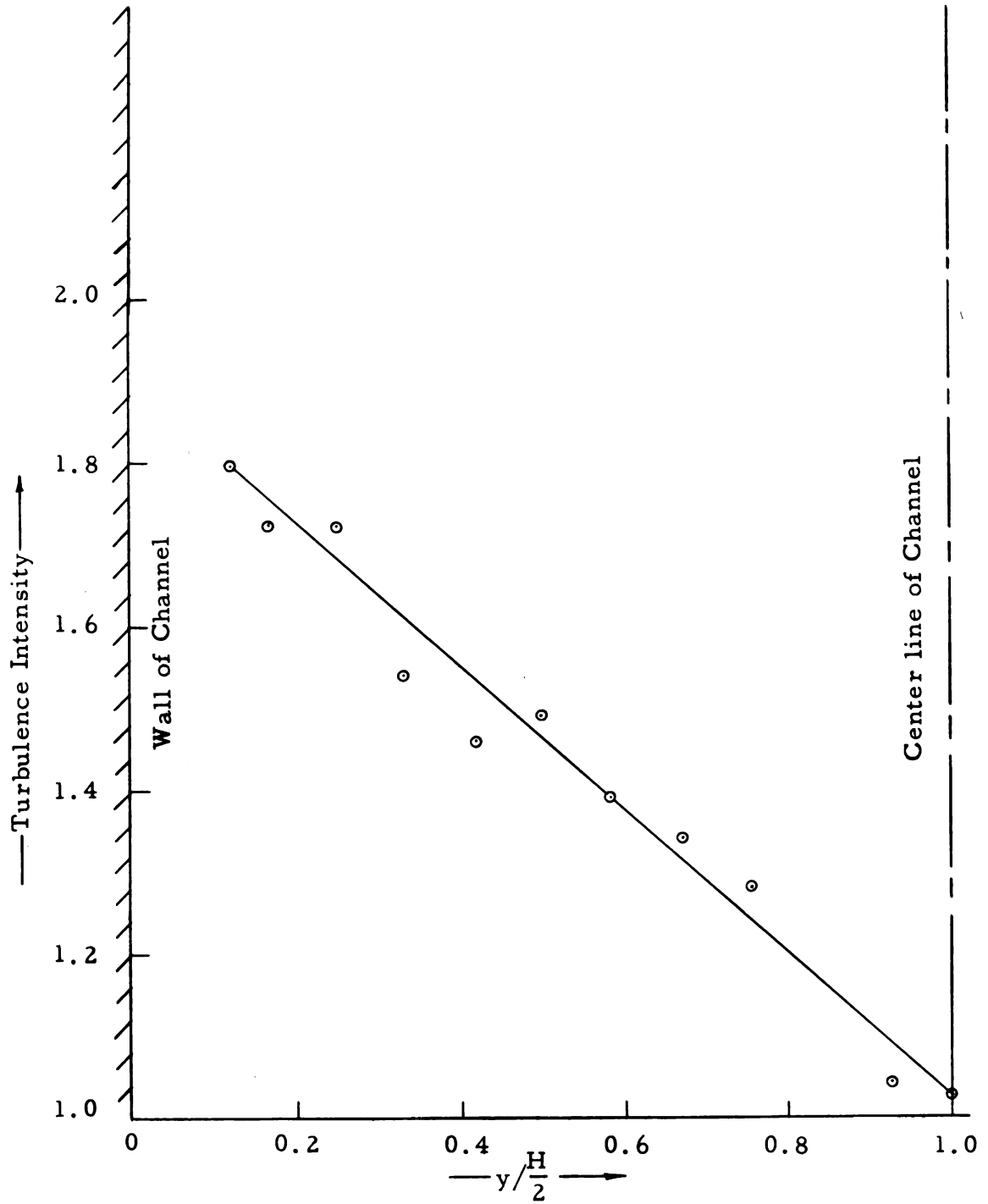


Figure 6. A typical velocity distribution in the testing section of the wind tunnel. Velocity is in ft./sec.

Figure 7. Measurement of turbulence intensity at the central plane normal to the flow in the testing section.



- (2) It should be possible to locate the filament at any desired angle, θ , around the cylinder.

Both of these objectives were met by the traverse mechanism used in the present investigation. The design of this mechanism is shown to scale in Figures 8 and 9, and its mechanics explained below.

The traverse mechanism is held to the circular disk F with a pin P so that there is no relative motion between them. However, the pin P can rotate freely in the plate G and the mahogany top of the cylinder H, thus, allowing rotation of the disk I and the traverse mechanism. The disk F is calibrated in degrees, and consequently allows the location of the filament at any desired angle, thus, satisfying the second requirement.

The blocks A and B are held tightly to plate D with screws. The shaft S passes through the plates A, B and C, and is secured to plate C with a set-screw, thus, preventing any rotation of the shaft. The tolerances for the shaft S are very small in the plates A and B, thus, preventing all movements of the shaft in either of the lateral directions. Therefore, the only motion possible for the shaft is in the longitudinal direction, and this is obtained by using the micrometer screw M held against plate C.

To reduce the vibration of the probe P, a stiffening rod R and another stiffener L were used. The cross section of the stiffening rod is shown in detail I. The probe P was held firmly inside the groove of the stiffening rod R with two screws in circular rings J and K. These screws pressed the probe P against the stiffener rod. The upper end of the stiffener R was threaded as shown in Figure 8.

The distance traversed by the filament was recorded with a dial indicator E impressed against the shaft S. To ascertain that this gave the actual distance traversed by the filament, another dial indicator was installed at O, and readings of both dial indicators taken for the cases of zero and maximum air velocities through the testing section. No discrepancy between the readings of the two indicators was noticed.

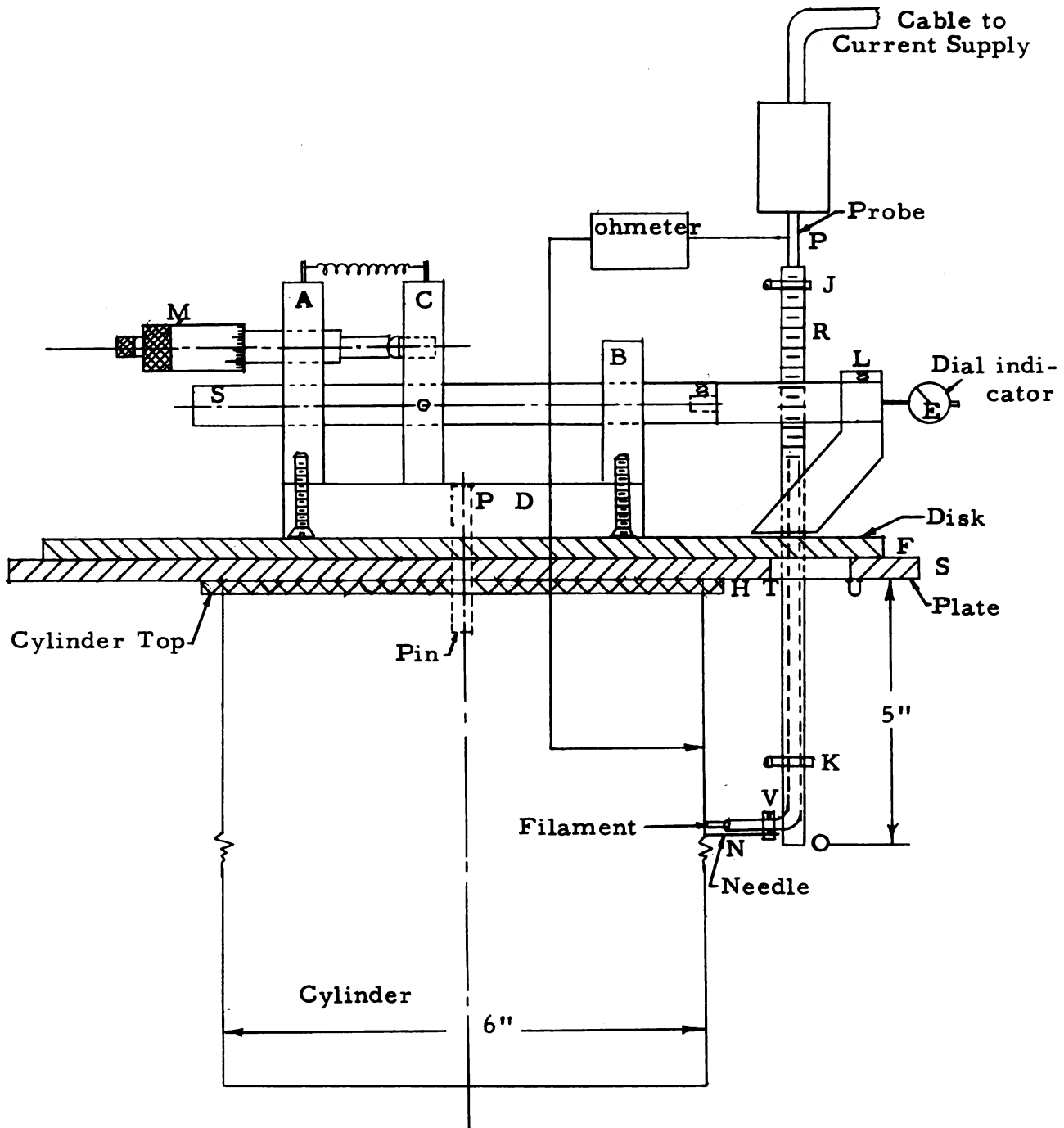


Figure 8. Elevation view of the traverse mechanism.

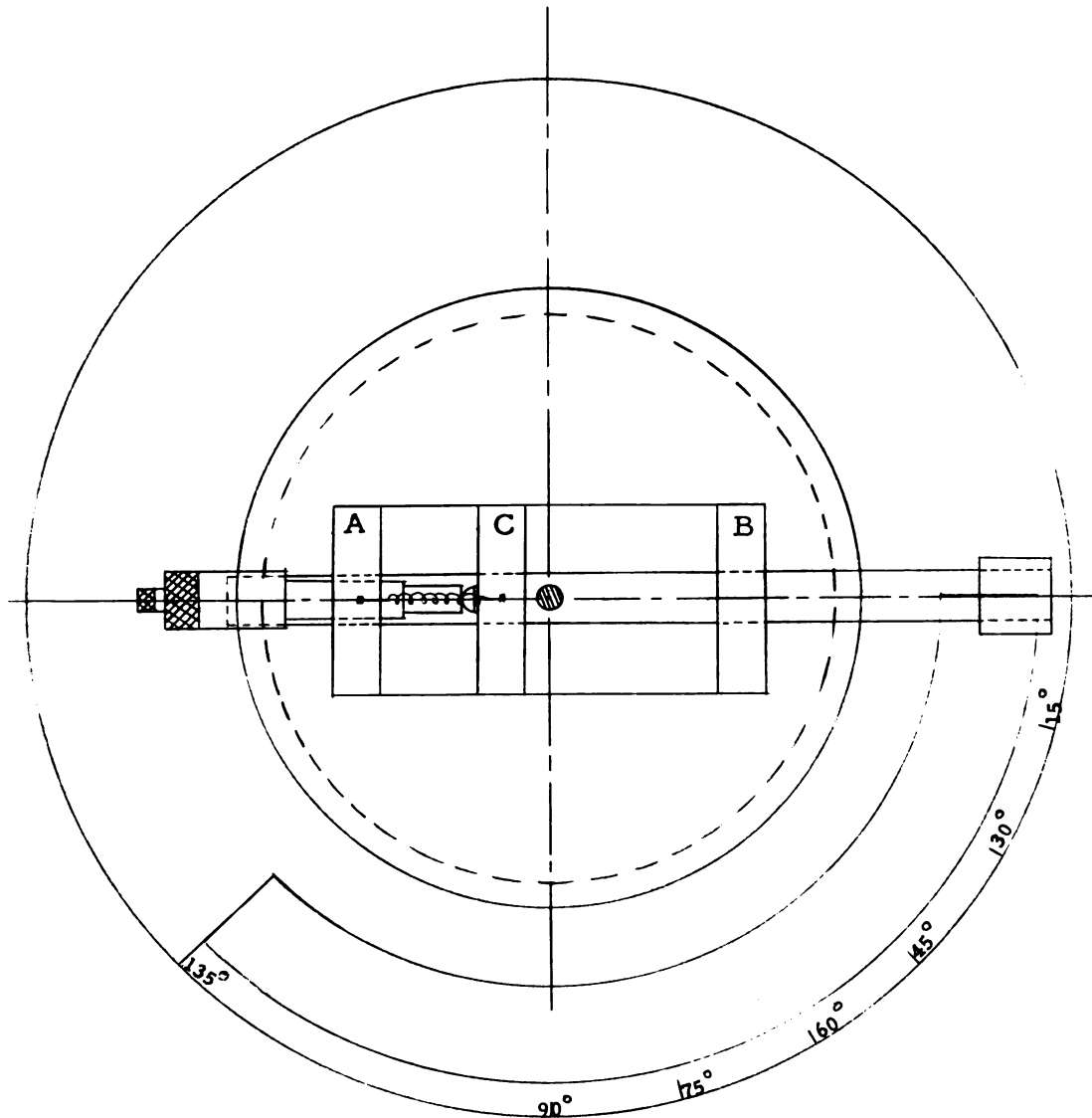


Figure 9. Plan View of the Traverse Mechanism.

The traverse mechanism described above provided an accurate method to locate the filament at any desired angle, and move it through any desired distance from its initial location. However, considerable difficulty was experienced in developing a method for an accurate, and predetermined initial location of the filament without its breakage. The method used in the present investigation met these requirements satisfactorily. A small attachment, V, was held to the probe with a set screw. The attachment carried an ordinary sewing needle. The attachment could slide along the probe tubing, and be held at any desired location. The distance between the filament and the needle tip was considered to be the initial location of the filament, when the needle just touched the cylinder, and this distance was determined by using a two dimensional measuring Pye microscope. The claimed accuracy was better than ± 0.01 mm. when moved over a full range of 20 cms. The next problem encountered was to determine when the needle N just touched the cylinder surface. When the needle tip and its image in the well polished brass surface of the cylinder just touched, it was regarded as indicative of the needle's just touching the cylinder. The results obtained with this method for the same conditions, but different runs were not consistent, and this method was given up in favor of using the electrical resistance method. An ohmeter, as shown in Figure 8, was connected between the cylinder and the probe. The contact of the needle with the cylinder completed the circuit, and a sudden change in the electrical resistance was observed on the ohmeter dial.

The hot wire anemometer probe used in the present investigation was a standard ten inch Flow Corporation probe. The probe tubing was bent in the Applied Mechanics laboratory. The filament was 0.0625 inch long and 0.00035 inch in diameter. The needle N was an ordinary sewing needle. The stiffening rod R was always at least 2 inches away from the cylinder and its effect on the boundary layer was discounted. The effect of the needle on the flow around the filament was regarded as negligible,

because the distance between the filament and the needle tip was of the order of 40 times the diameter of that part of the needle which was inside the boundary layer.

The Turbulence Grids and Intensity Measurement

1. The Turbulence Generating Grids

The intensity and scale of turbulence in the free stream in the testing section were varied by using a number of bi-plane grids as shown in Figure 10B. The mesh length M , the distance between the centers of two adjacent bars was held constant at one inch, while the bar diameter was changed. The diameters of the circular bars were 0.068", 0.190", 0.329" and 0.50". The grids were located nineteen inches ahead of the cylinder. The investigation of Bains and Patterson [2] indicates that turbulence becomes isotropic at a distance of about $10M$ downstream from the turbulence generating grids. Therefore, it could be safely assumed that turbulence in the testing chamber of the wind tunnel was isotropic.

2. Turbulence Intensity Measurement

The instructions given in reference [9] were followed in determining the turbulence intensity. Figure 10A shows the various instruments used excluding the probe already described in Figure 8. The instruments have been assigned numbers for identification, and will be referred to in the following discussion. The signal from the hot wire anemometer amplifier (1), was fed to the attenuator lying on the top of (1). This attenuator was used to satisfy the requirement for using the Ballantine root mean square r.m.s.) meter (4). The requirement was that the crest value (ratio of peak to peak amplitude to r.m.s. amplitude of a non-sinusoidal signal) must not be greater than five. When the crest value was greater than five,

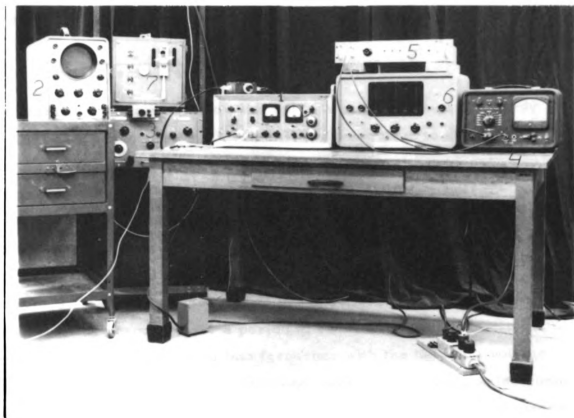


FIGURE 10A. Various instruments (excluding the hot wire anemometer probe) used during the present investigation.

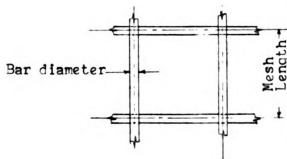


FIGURE 10B. A section of a typical turbulence generating grid.

an attenuator should be used in series with the r.m.s. meter; so that the maximum reading on the r.m.s. meter did not exceed a value of

$$\frac{5}{\text{Crest Value}} \times \text{Full Scale Reading}$$

The signal from the attenuator was fed to a pair of Spencer-Kennedy variable electronic filters (3). The filters were used to allow the frequency band of 25-20,000 cps, thus eliminating the extraneous wave discussed in Section III A, and high frequency amplifier noise.

The readings taken from the r.m.s. meter for the noise level with turbulent fluctuations superimposed on it were very unstable, and it was extremely difficult to read mean values, although the response time of the r.m.s. meter was increased to 2.5 seconds. To obtain an average of the fluctuating readings over a period of about 2 minutes, the r.m.s. meter voltage was converted into frequency with the help of a voltage-frequency converter (5). This frequency was recorded on an electronic counter (6) for the desired time with open gate. The voltage-frequency calibration curves for various scales of the voltage-frequency converter used in the present investigation are shown in Figures 11 and 12.

Determination of Velocity Profiles

Theoretical [15] as well as experimental [16] studies of the heat transfer from a cylinder to air or liquids flowing normal to the cylinder axis have led to certain relationships between the heat transfer and the flow velocities that form the basis of using hot wire anemometry in determining the velocity and its fluctuations at any point in the flow.

By using Kramer's empirical relationship for the coefficient of heat transfer, the expression (4) for the heat transferred per unit time, H , from a filament of length l to the ambient gas or liquid due to forced convection has been derived in Chapter 2 of reference [13].

Figure 11. Calibration curve (voltage vs. frequency) for the voltage to frequency converter.

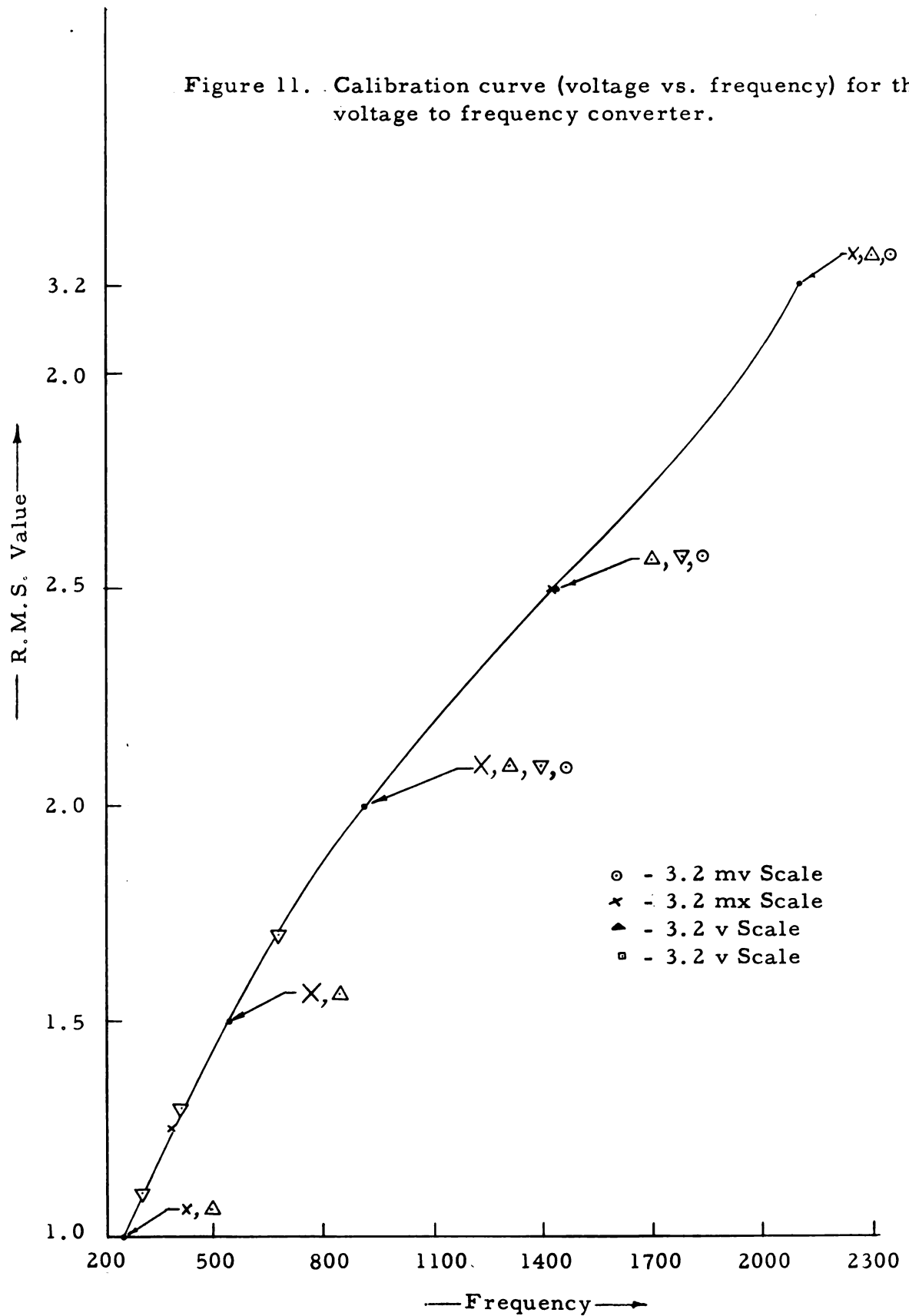
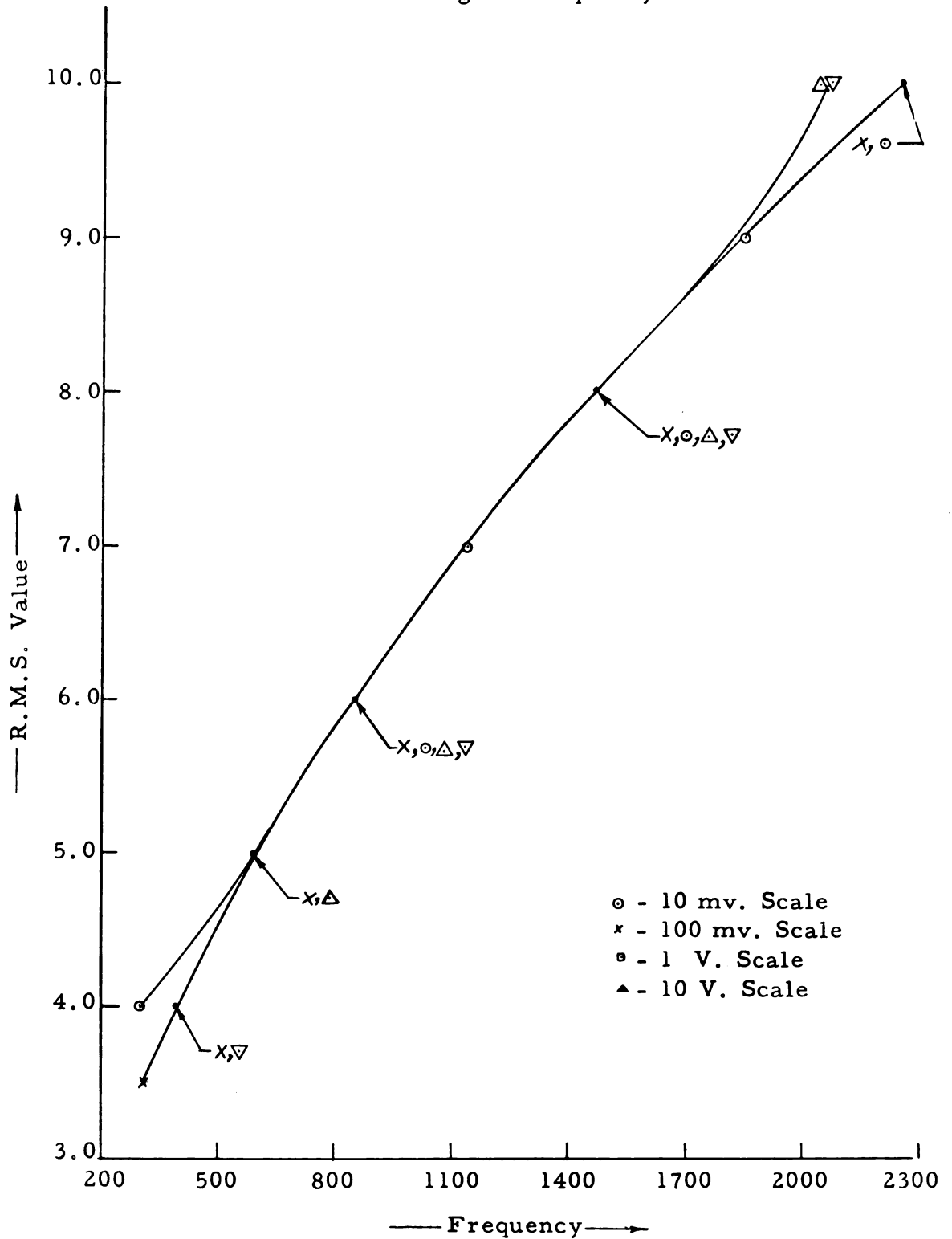


Figure 12. Calibration curve (voltage vs. frequency) for the voltage to frequency converter.



$$H = A + B \sqrt{U} \quad (4)$$

Where A and B are factors that depend on the filament as well as on the flow. The assumptions made in deriving equation (4) are

- (1) The filament is a circular cylinder.
- (2) The filament has uniform temperature.
- (3) No heat is transferred from the filament to the fluid through mechanisms other than forced convection.
- (4) All the terms of order 2 or higher in the expression for temperature dependence of the electric resistance of the filament can be neglected.
- (5) Reynolds number based on the diameter of the filament and local velocity should be greater than 0.01 and less than 10,000.

For thermal equilibrium conditions, this heat loss must be equal to the heat generated per unit time by the electric current through the wire, i. e., it must be equal to $I^2 R_w$ where I is the electric current and R_w the total electrical resistance of the wire. Thus,

$$I^2 R_w = A + B \sqrt{U} \quad (5)$$

In the practice of hot wire anemometry the factors A and B are determined experimentally. For a constant temperature of the filament, i. e., for a constant electric resistance of the wire, the relation between I^2 and \sqrt{U} must be linear, according to equation (5). This linearity is satisfactorily confirmed by experiment, as shown in Figure 14. The values of A and B can then be determined from the graph shown in this figure.

As stated earlier, equation (4) is valid only when the heat is transferred from the filament to the ambient gas through forced convection only. However, heat transfer may not be completely through forced convection when the filament is located very close to a surface. The presence of a surface very close to the filament has two effects. First, the flow pattern

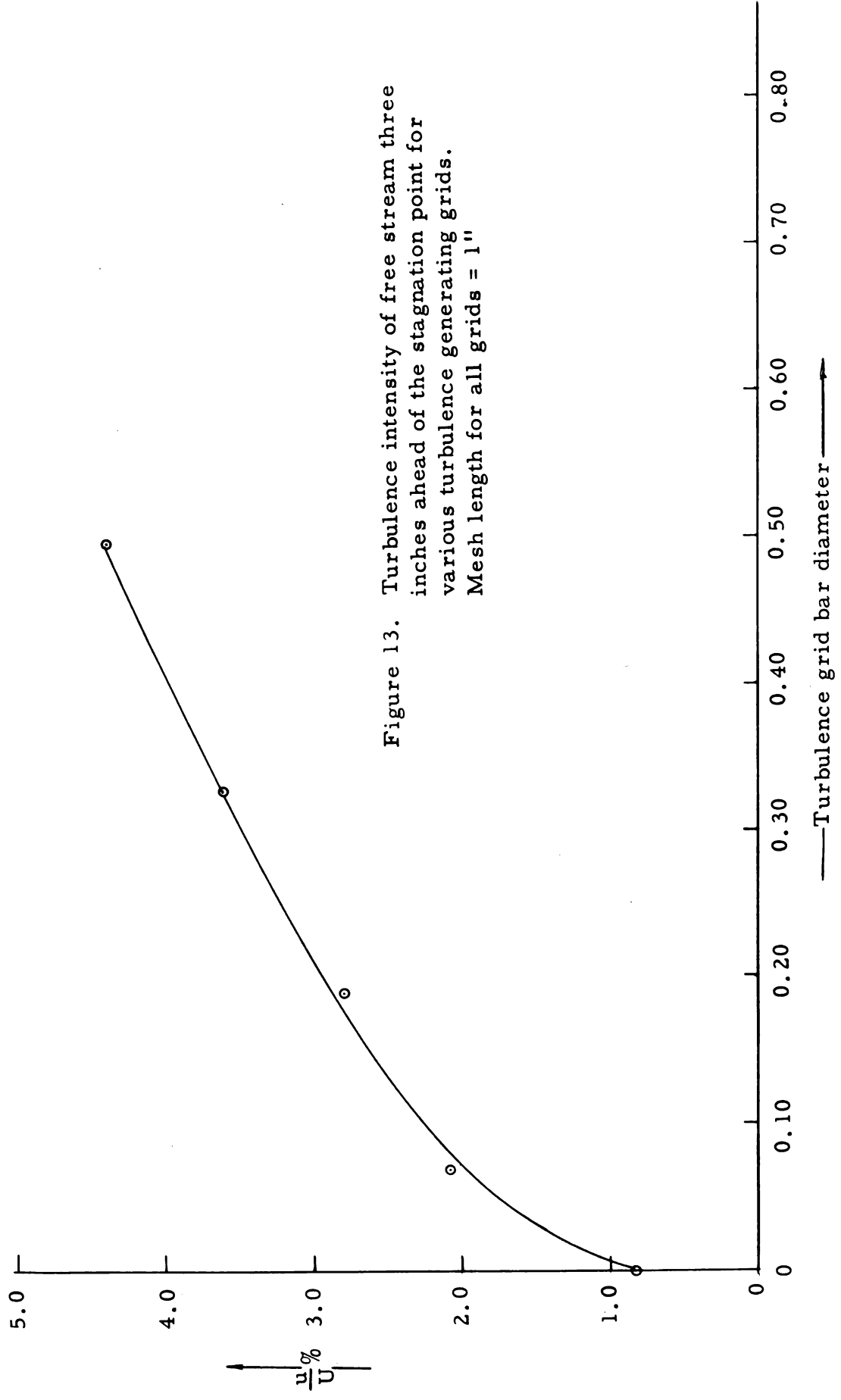


Figure 13. Turbulence intensity of free stream three inches ahead of the stagnation point for various turbulence generating grids. Mesh length for all grids = 1"

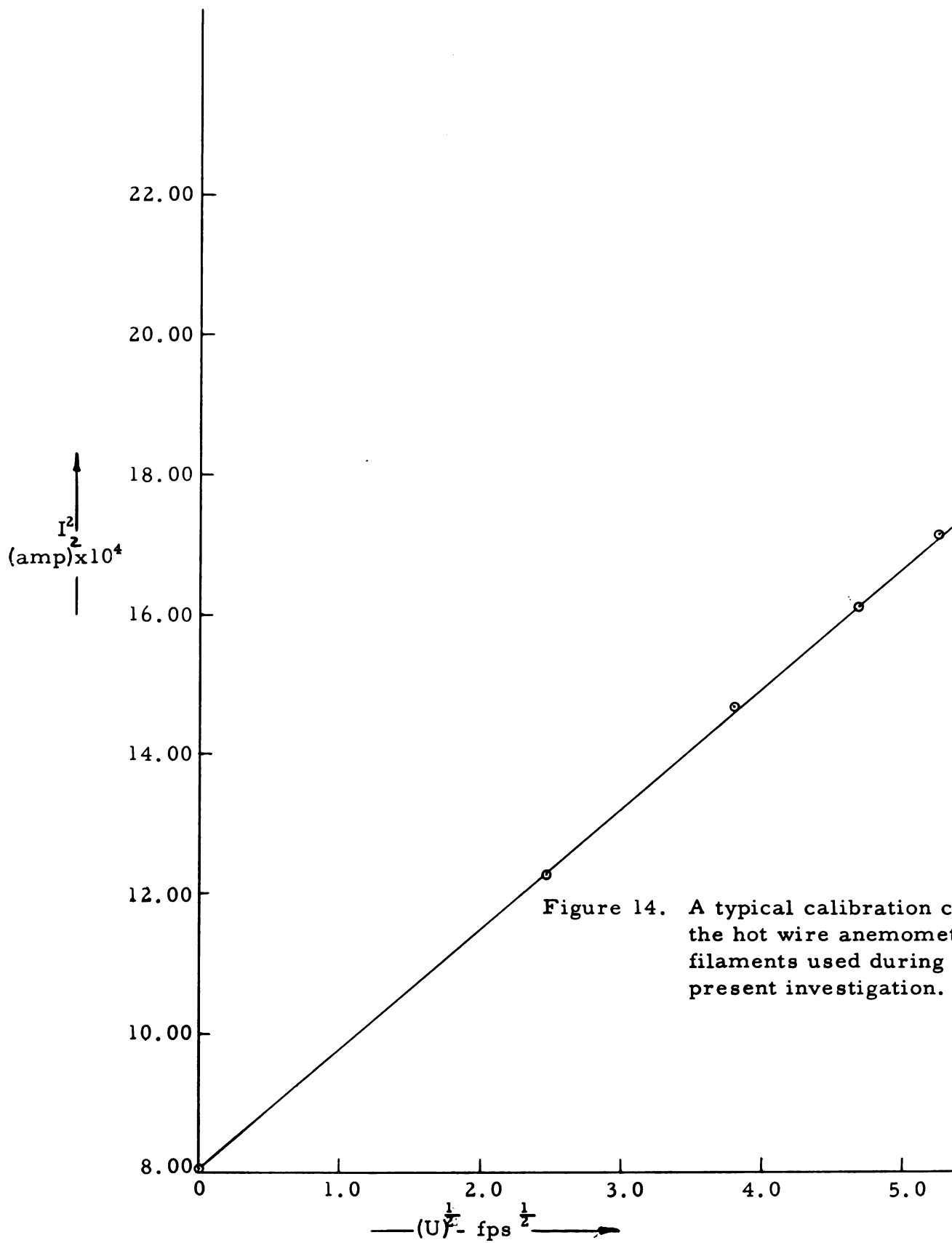


Figure 14. A typical calibration curve for the hot wire anemometer probe filaments used during the present investigation.

around the filament may be modified, and secondly, a fraction of the heat may be transferred to the surface through, possibly, all modes of heat transmission. Concerning the first effect, no work seems to have been done. However, several investigators have endeavored to determine the heat loss to the surface by conducting an experiment in still air at several wire temperatures to find the difference between the rate of heat loss near the surface, and that far from the surface. In this manner, the heat loss is found as a function of the wire temperature and the distance from the surface. Dryden [5] found the heat loss to an aluminum plate as

$$H_p = 1.27 (10)^{-8} \frac{l}{y} (\Delta T)^2 \quad (6)$$

where

H_p = The heat loss to the plate, in watts

y = The distance from the plate, in inches

l = Length of the filament, in inches

ΔT = The temperature difference between the wire and the plate, °C.

Recently Wills [28] has investigated experimentally the corrections for hot-wire readings for proximity to a solid boundary. From the results presented in reference [28], it can be concluded that the corrections needed for the present investigation are negligible.

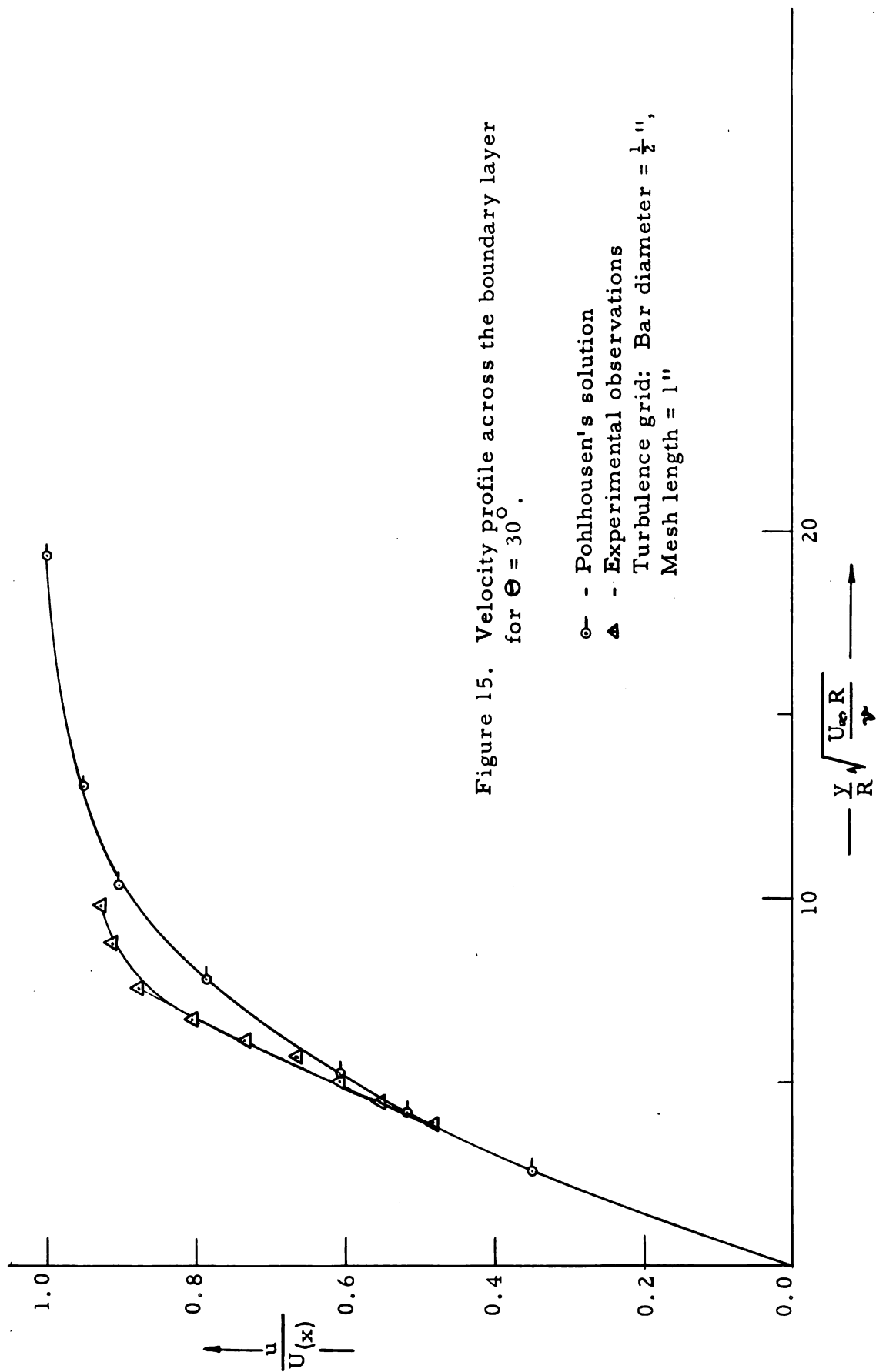
For the filament in use at the time of observations a calibration curve (I^2 vs $U^{\frac{1}{2}}$) was obtained every day. A pitot tube and the hot wire probe were located side by side, and the velocities and the currents were measured. The currents were fed to a filament and measured according to the instructions in reference [9]. To obtain a velocity profile in the boundary layer, the filament was located at various points, and currents recorded. From these known values of current at various locations the corresponding velocities were obtained through the most recent calibration curve for the particular filament in use.

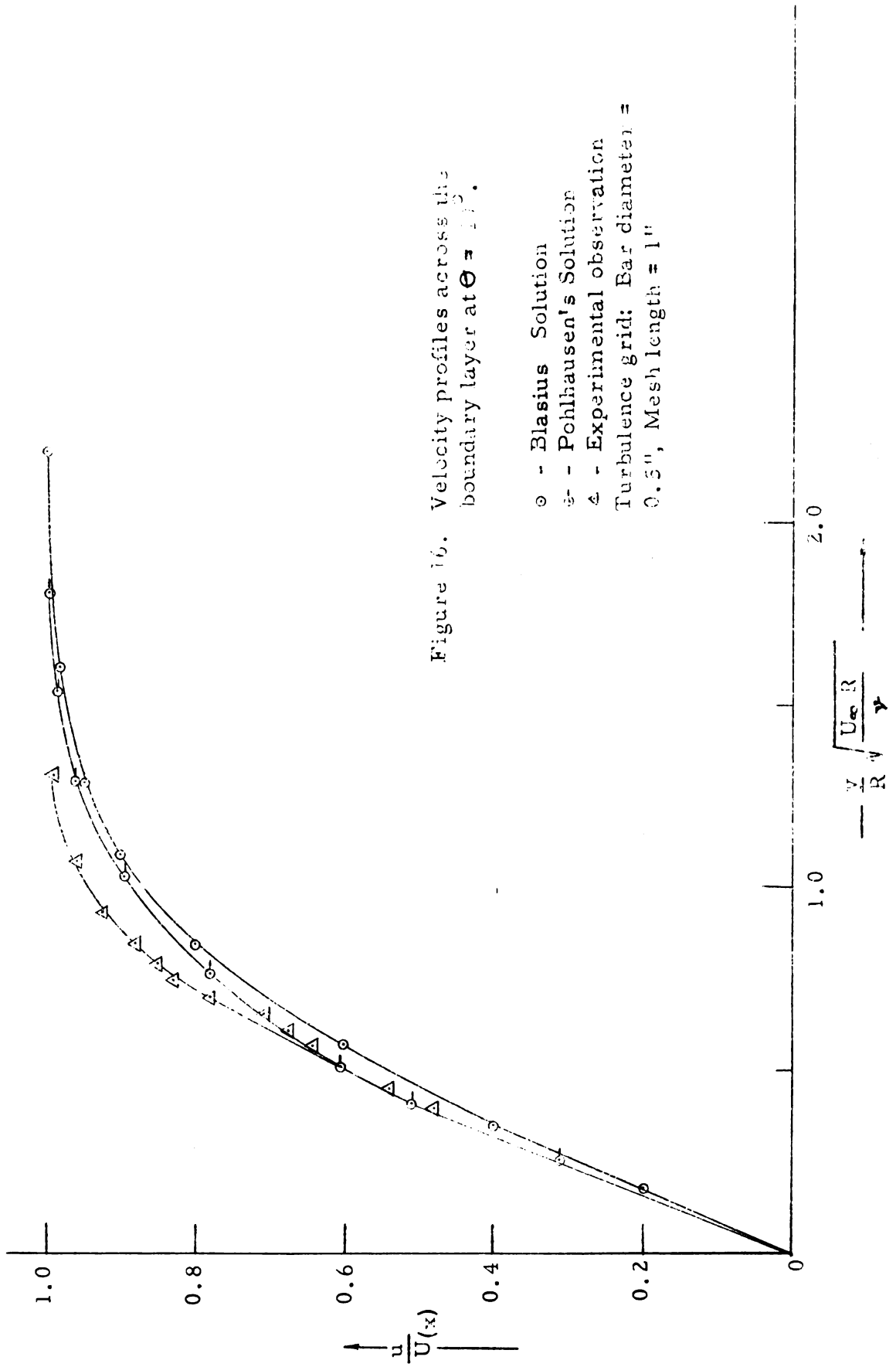
Since the Blasius velocity profiles in the laminar boundary layer around a circular cylinder at various angles from the stagnation point are known, it was decided to obtain velocity profiles experimentally at some locations and compare them with the Blasius profiles. This was done to investigate the accuracy of the traverse mechanism, and also to gain experience in using the hot wire anemometer. Some typical velocity profiles are shown in Figures 15, 16, and 17. In these graphs it can be noticed that the experimental profiles are steeper than the theoretical ones. Data was taken for several other angles, as well as repeated for some angles. For all the angles, the extra steepness of the experimental profiles in the outer part of the boundary layer was noticed. Furthermore, it was also observed that the data reproduced itself excellently with a maximum deviation of only 3%.

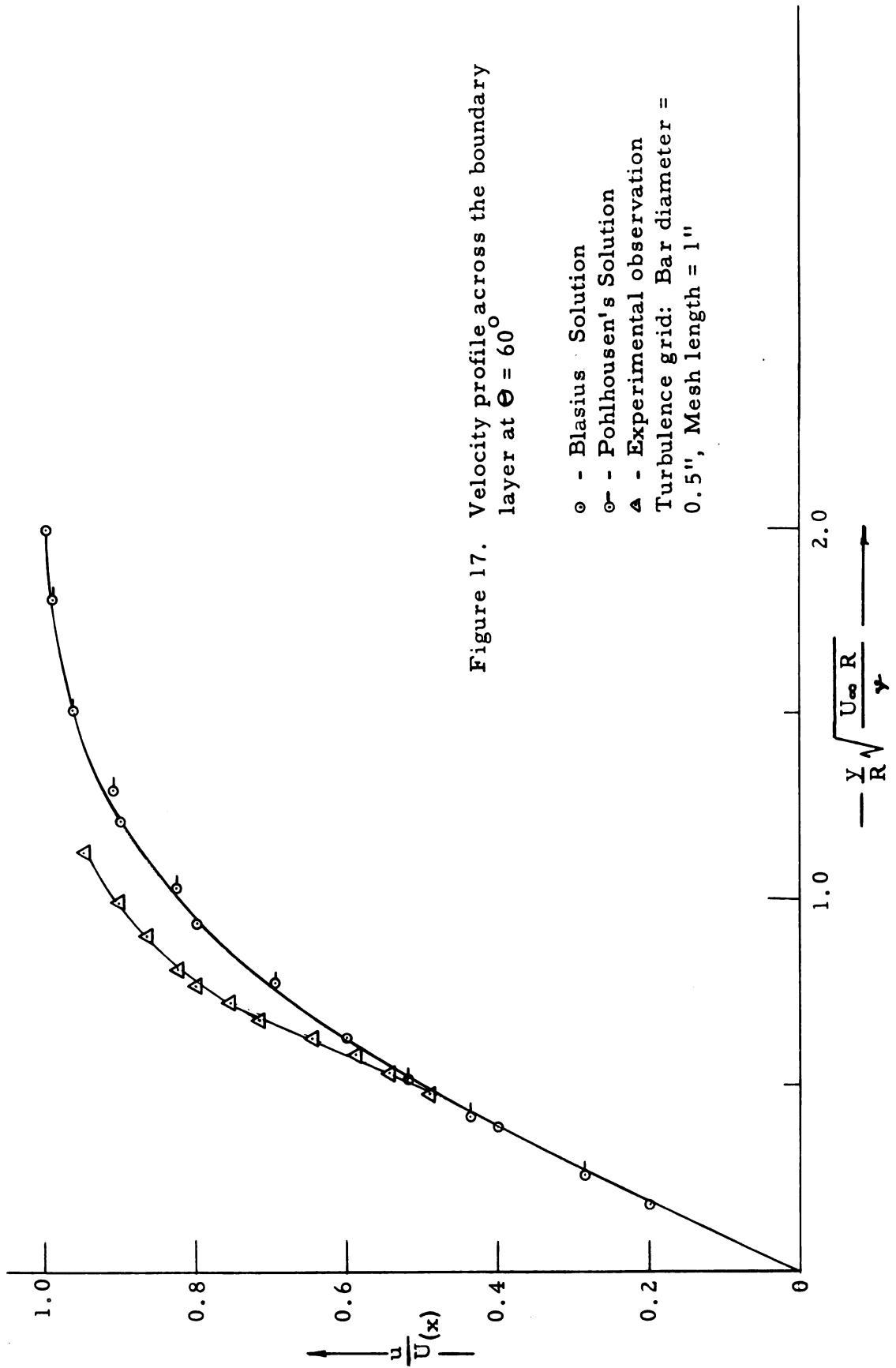
It was decided to investigate into the causes for the steepness. Various physical factors that could possibly have an effect were modified. The physical factors considered here were:

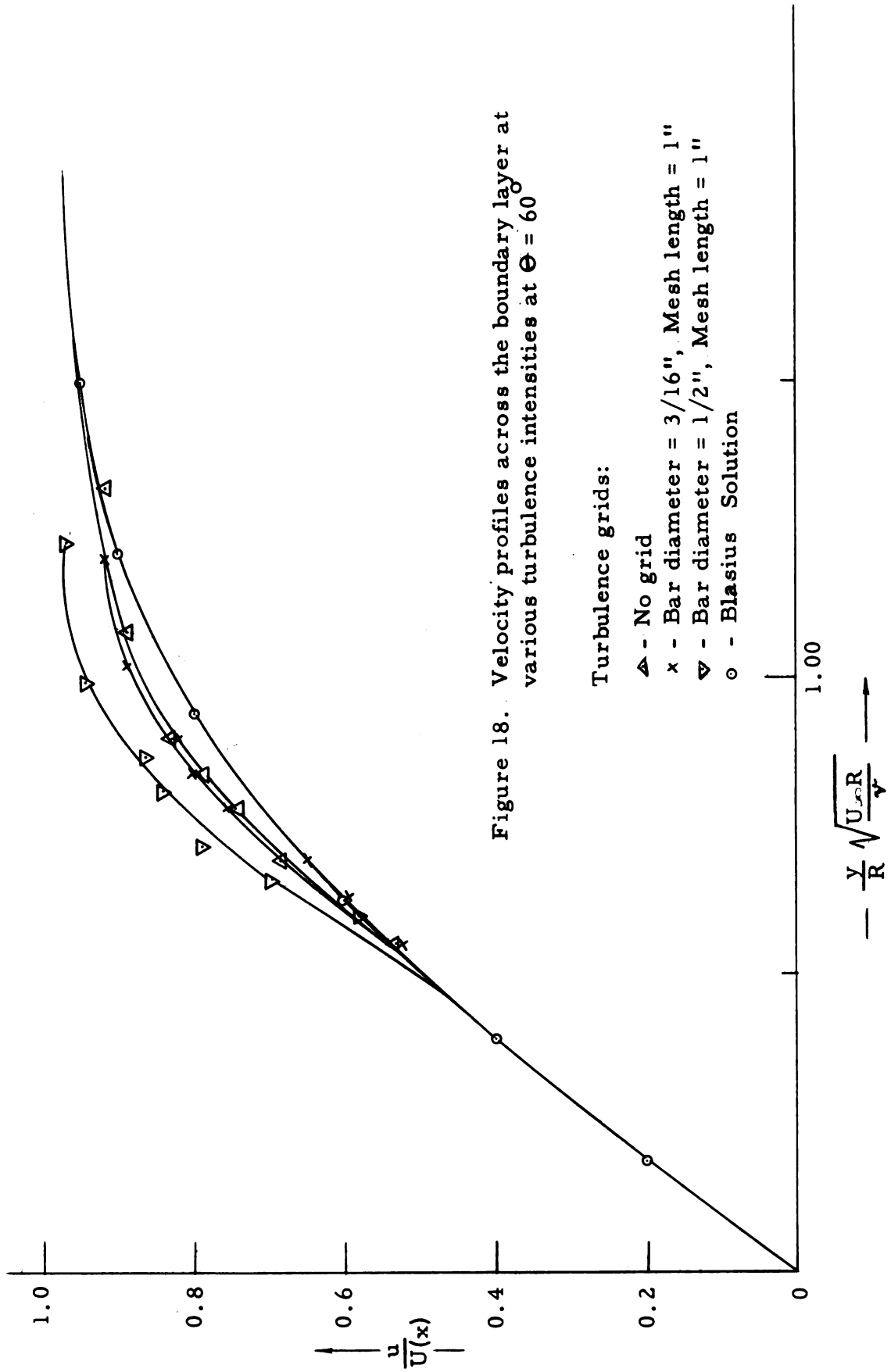
- (1) The cylinder material was changed. Cylinders of the same diameter made of brass and plastic were used.
 - (2) The cylinder surfaces were polished.
 - (3) The vibration of the probe was reduced by using the stiffener L, as shown in Figure 8.
 - (4) The distance between the needle tip and the filament observed with the microscope was confirmed with feeler gauges.
 - (5) The observations of the dial indicator E were checked with another dial indicator located at point 0.
 - (6) The cylinder was set so that the angle of attack was 0° .
- Furthermore, it was also decided to obtain Pohlhausen's solution.

The above mentioned factors and the Pohlhausen's solution had no noticeable effect on the steepness of the experimental curves. Finally, it was decided to investigate the effect of turbulence intensity. The velocity profiles were observed under three conditions of turbulence intensity.









These turbulence conditions were achieved (1) without a grid, (2) 3/16" diameter bar grid with $M = 1''$, and (3) 1/2" diameter bar grid with $M = 1''$. The results are shown in Figure 18.

It can be seen clearly from Figure 18 that the effect of an increase in the turbulence intensity is to cause the velocity profile to be steeper. The most probable reason for this phenomenon was considered to be the diffusion of turbulence into the outer part of the boundary layer.

Determination of Pressure Coefficient Distribution

Pressure coefficient, C_p , at any point is the ratio of the excess of the local static pressure, $p_0 + p'$, over the free-stream static pressure, p_0 , to the free stream velocity pressure, $\frac{\rho U_\infty^2}{2}$. Using Bernoulli's equation the following relationship can be derived:

$$C_p = \frac{\frac{\rho}{2} (U_\infty^2 - U_{(x)}^2)}{\frac{\rho U_\infty^2}{2}} \quad (7)$$

where $U_{(x)}$ is the local fluid velocity just outside the boundary layer for the case of fluid flow in the proximity of a solid surface. It is considerably important to know the pressure coefficient distribution around the circular cylinder used in the present investigation for various turbulence intensities because, the properties of the boundary layer depend strongly on such distributions [22]. It may be remarked here that the purpose of the present investigation was to study not the boundary layer along the surface of a circular cylinder, but rather the boundary layer on a surface with a known pressure coefficient distribution.

The circular cylinder used during the present investigation had static pressure openings located at intervals of ten degrees accurately. Small copper tubes, connected to inclined multimanometers through flexible plastic tubing, led to the pressure openings in the cylinder and were flush

with the cylinder surface. A petroleum oil with specific gravity of 0.834 was used as the manometric fluid. With this set-up the static pressure distributions were obtained in terms of inches of oil. With manometers inclined at the same angle the free stream velocity pressures for various conditions of turbulence intensity were measured with a pitot tube in the absence of the cylinder. The value of $\frac{\rho U(x)^2}{2}$ at any point for a given condition was obtained by subtracting the local static pressure from the pressure at the stagnation point for the same condition of flow.

CHAPTER IV

PRESENTATION AND DISCUSSION OF RESULTS

Coefficient of Pressure Distribution

For a non-viscous fluid with constant density and no body force the distribution of the coefficient of pressure around a circular cylinder can be expressed by equation (8) as derived in reference [29].

$$C_p = \frac{p'}{p_n} = 1 - 4 \sin^2 \Theta \quad (8)$$

where

C_p = Coefficient of Pressure

$$p_n = \frac{\rho U_\infty^2}{2}, \text{ in lb}_f\text{ft}^{-2}$$

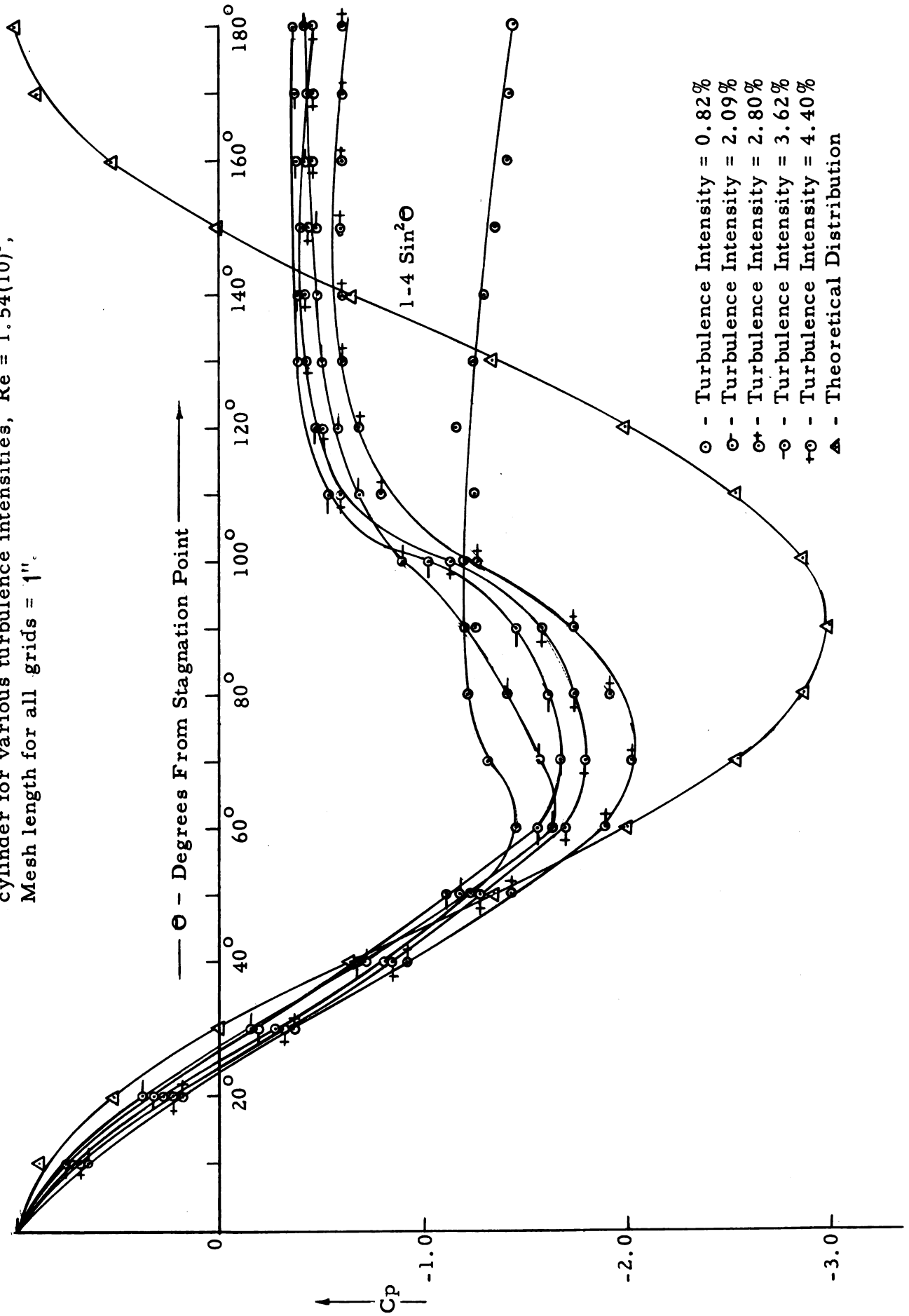
p' = Excess of local static pressure, $p_0 + p'$,
over the free stream static pressure, p_0 ,
in $\text{lb}_f\text{ft}^{-2}$

Θ = Angle from the stagnation point, in degrees.

The distribution expressed by equation (8) is shown in Figure 19. The distributions of the coefficient of pressure for various turbulence intensities at Reynolds number of $1.54(10)^5$ around the cylinder used in the present investigation are also shown in Figure 19.

The deviation of experimental results from the distribution for an ideal fluid is caused chiefly by the fluid viscosity. It can also be observed from Figure 19 that changes in the free stream turbulence intensity also have considerable effect on the distribution of the coefficient of pressure.

Figure 19. Coefficient of pressure distributions around the circular cylinder for various turbulence intensities, $Re = 1.54(10)^5$, Mesh length for all grids = 1".



Intensity of Skin Friction Distribution

The intensity of skin friction, $(\frac{C_f}{2})$, at a surface due to fluid flow along the surface can be expressed by equation (9).

$$\left(\frac{C_f}{2}\right) = \mu \left(\frac{\partial u}{\partial y}\right) / \frac{1}{2} \rho U_\infty^2 \quad (9)$$

The results of the intensity of skin friction measurements made during the pressure investigation for various free stream turbulence intensities at a Reynolds number of $1.54(10)^5$ are represented in Figures 20 to 24. These figures also contain the theoretical distribution of skin friction due to Blasius [22], and the experimental distribution due to Giedt [12] for the purpose of comparison.

The agreement between the results of the present investigation and those of Blasius and Giedt is good up to $\Theta = 60^\circ$ for all cases. Fage and Faulkner [2] observed a sharp minimum in the vicinity of $\Theta = 85^\circ$ after which the skin friction intensity increased till a sharp maximum was reached. After this maximum the skin friction intensity decreased gradually up to the point of separation of the boundary layer where the skin friction intensity becomes zero. Fage and Faulkner interpreted the points of minimum and maximum as the start and the end of the transition region respectively. During the present investigation a sharp minimum and a sharp maximum as described above were not observed. However, large fluctuations in the skin friction intensity curves were observed in the transition region. These fluctuations do not represent the scattering of data because, the fluctuations were observed even when the data was taken several times. It is believed that these fluctuations were produced by the random appearance of turbulence spots. It should be noted that, for the present investigation, a hot wire anemometer was used, while Fage and Faulkner employed a surface tube. These fluctuations have not been observed either by Fage and Faulkner or Giedt. The probable reasons for

Figure 20. Skin Friction distributions around a circular cylinder.

∇ - Blasius distribution, $Re = 1.54(10)^5$, Turbulence Intensity = 0.0%
 \blacktriangle - Present investigation, $Re = 1.54(10)^5$, Turbulence Intensity = 0.82%
 \circ - Giedt's investigation, $Re = 1.66(10)^5$, Turbulence Intensity $\approx 1.0\%$

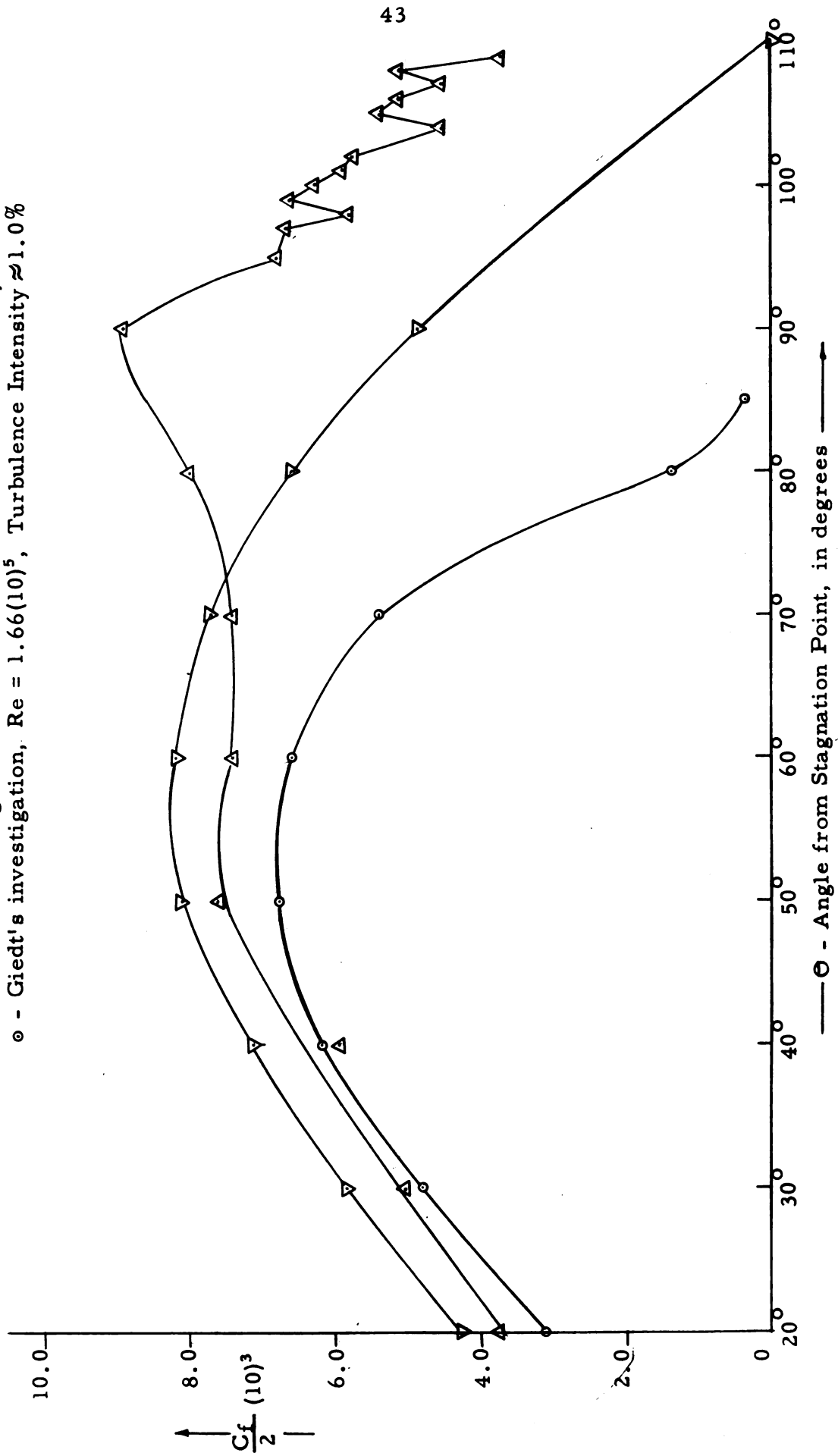


Figure 21. Skin Friction distribution around a circular cylinder.

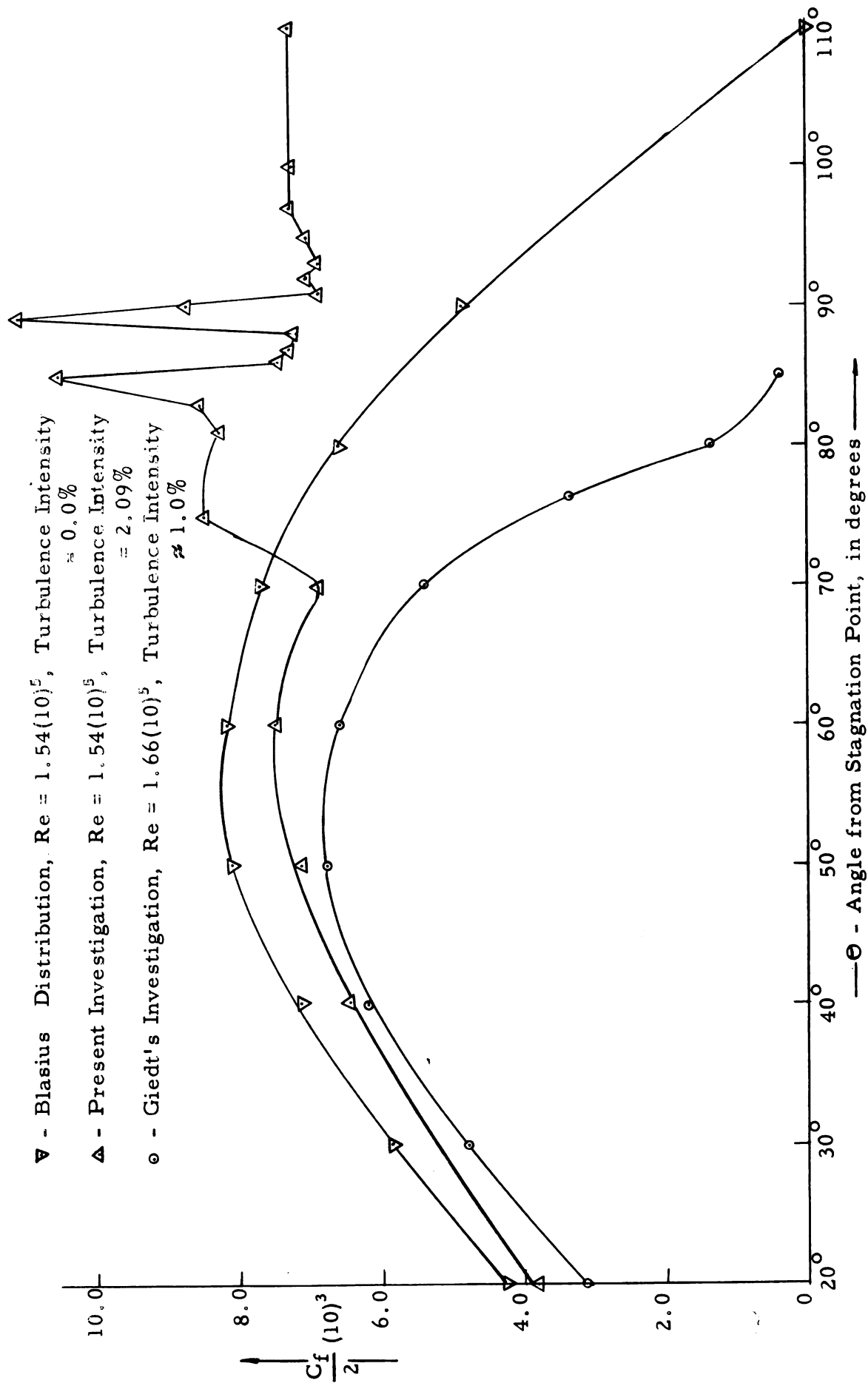
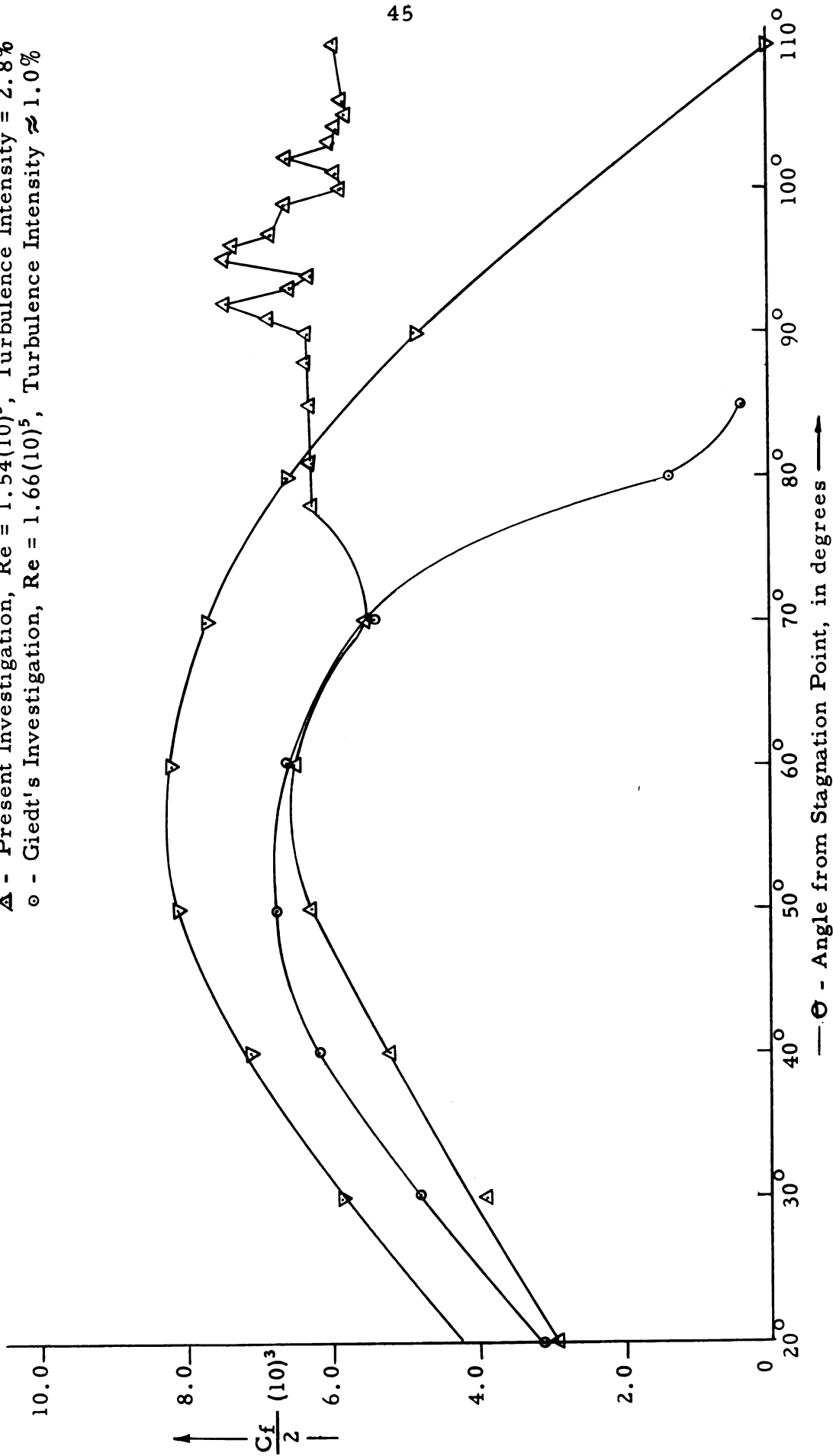


Figure 22. Skin Friction distributions around a circular cylinder.

- ▽ - Blasius Distribution, $Re = 1.54(10)^5$, Turbulence Intensity = 0.0%
- △ - Present Investigation, $Re = 1.54(10)^5$, Turbulence Intensity = 2.8%
- - Giedt's Investigation, $Re = 1.66(10)^5$, Turbulence Intensity ≈ 1.0%



○ - Angle from Stagnation Point, in degrees →

Figure 23. Skin Friction distributions around a circular cylinder.

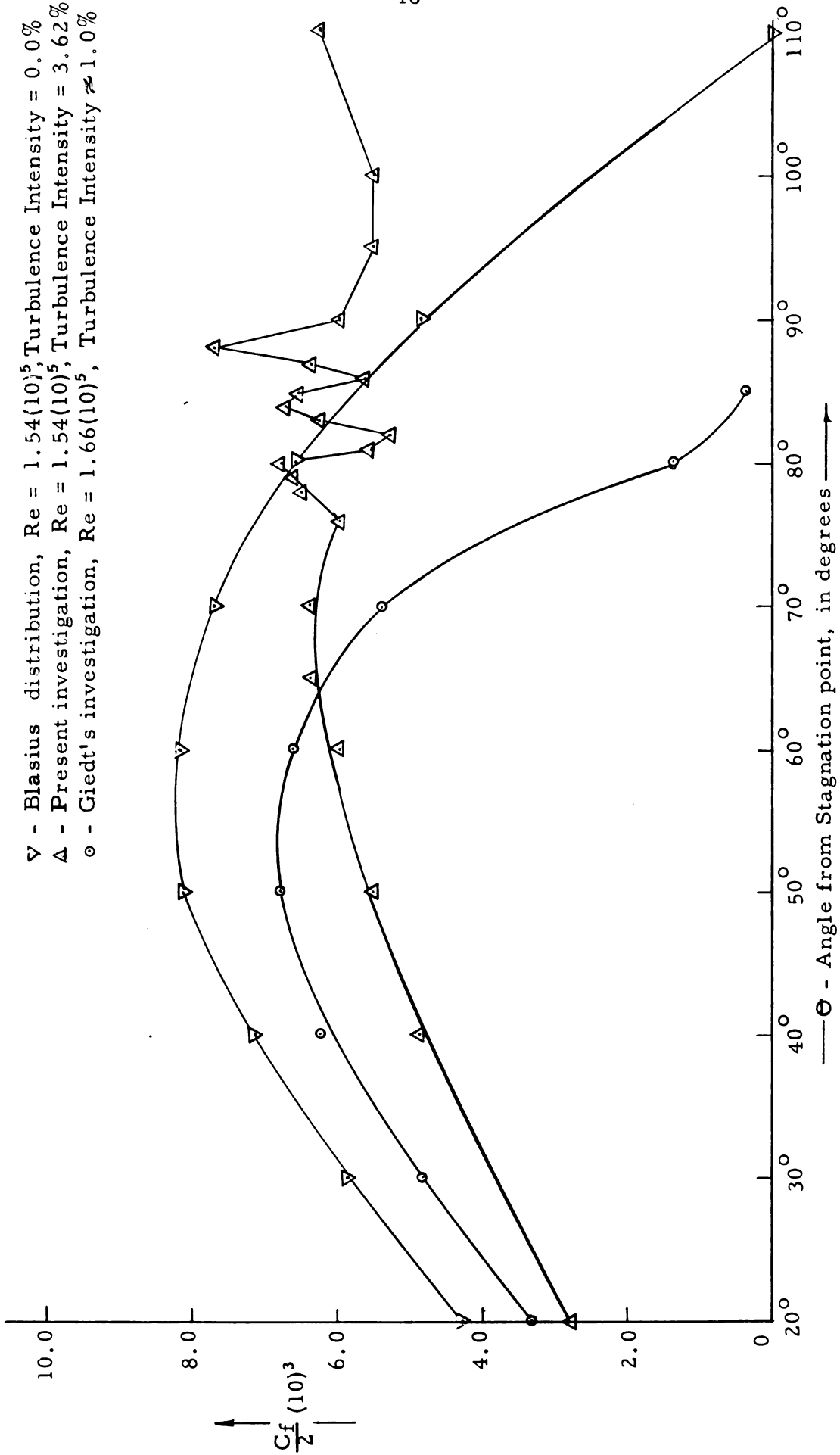
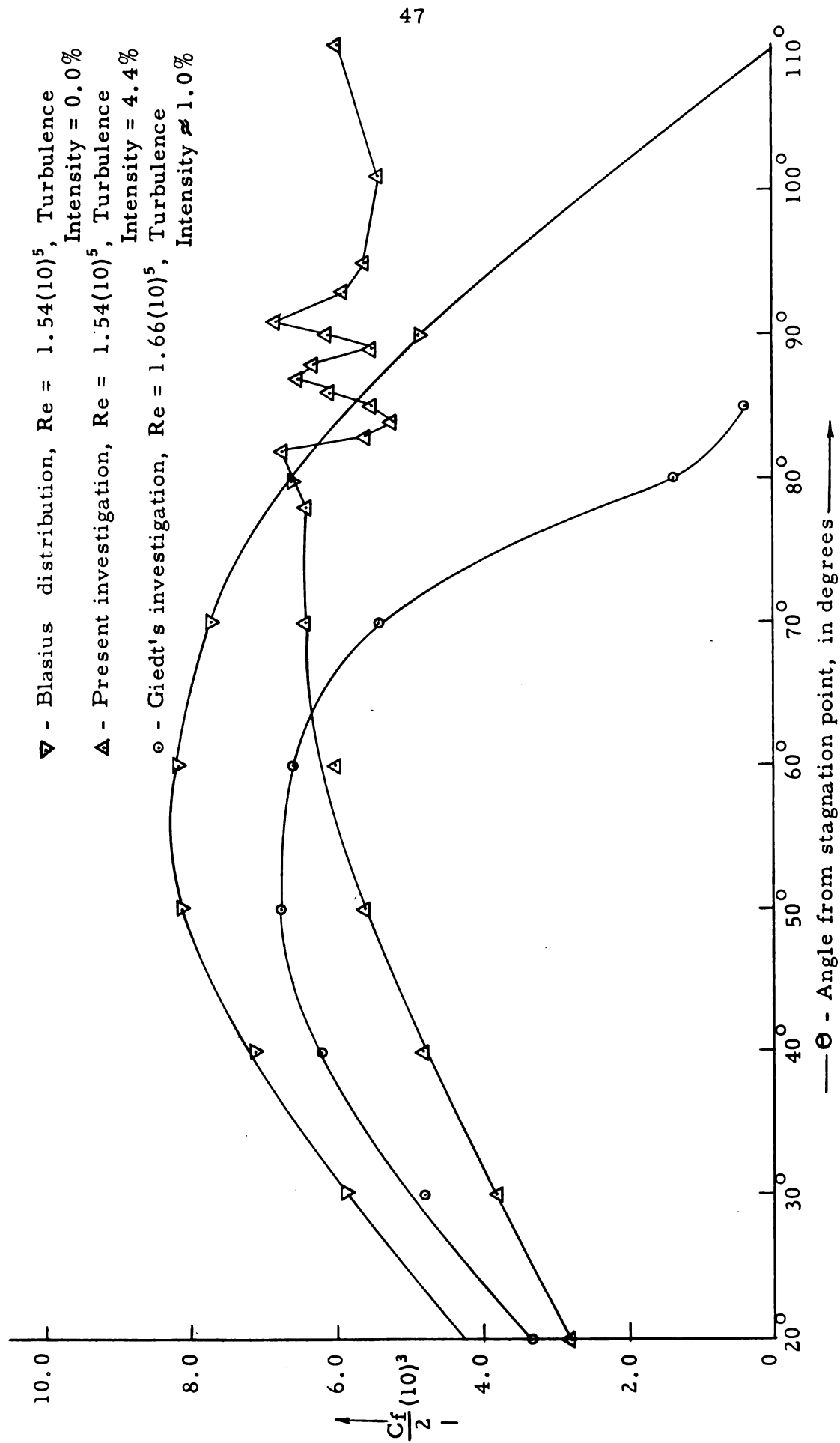


Figure 24. Skin Friction Distributions Around a Circular Cylinder

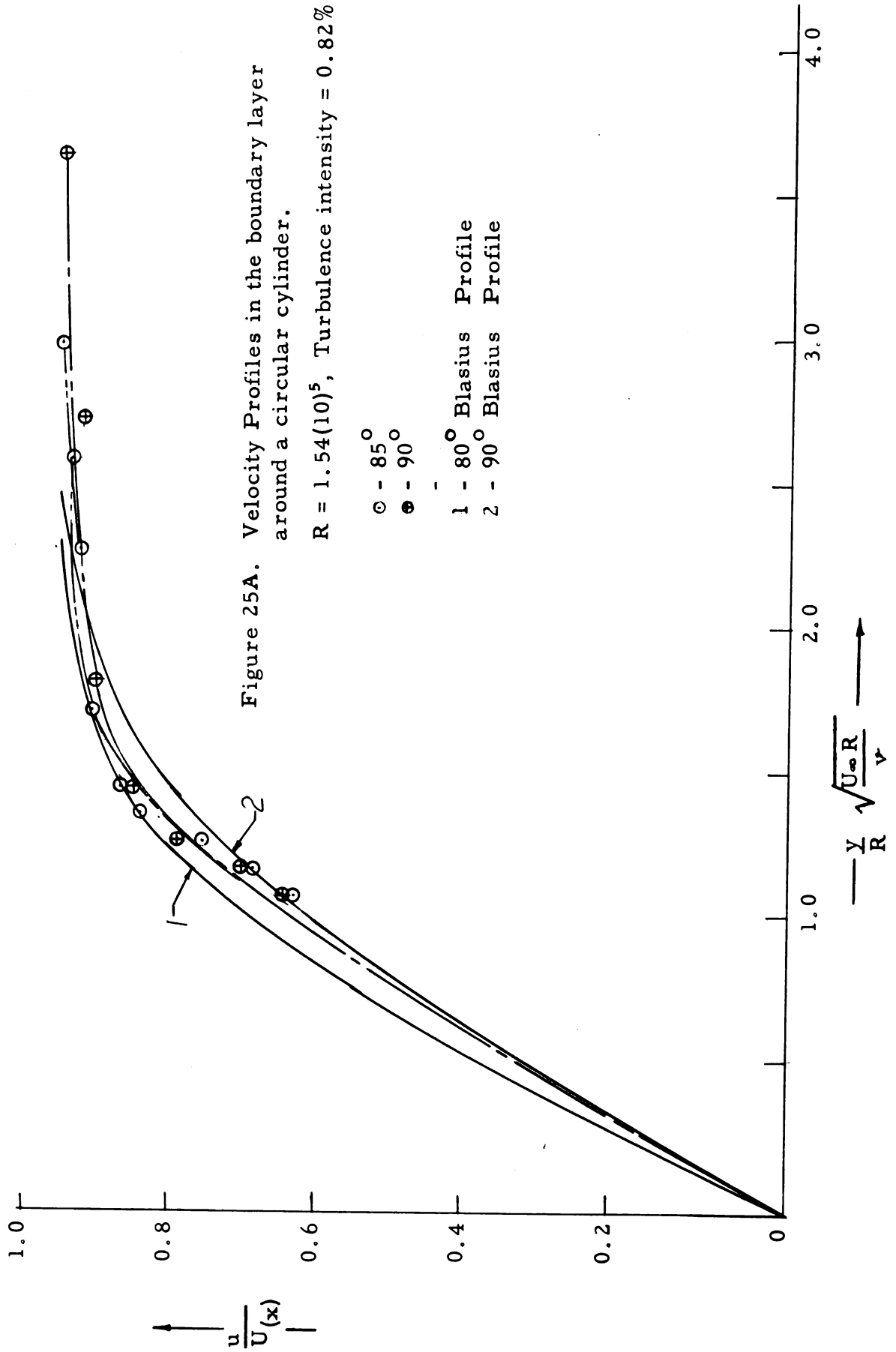


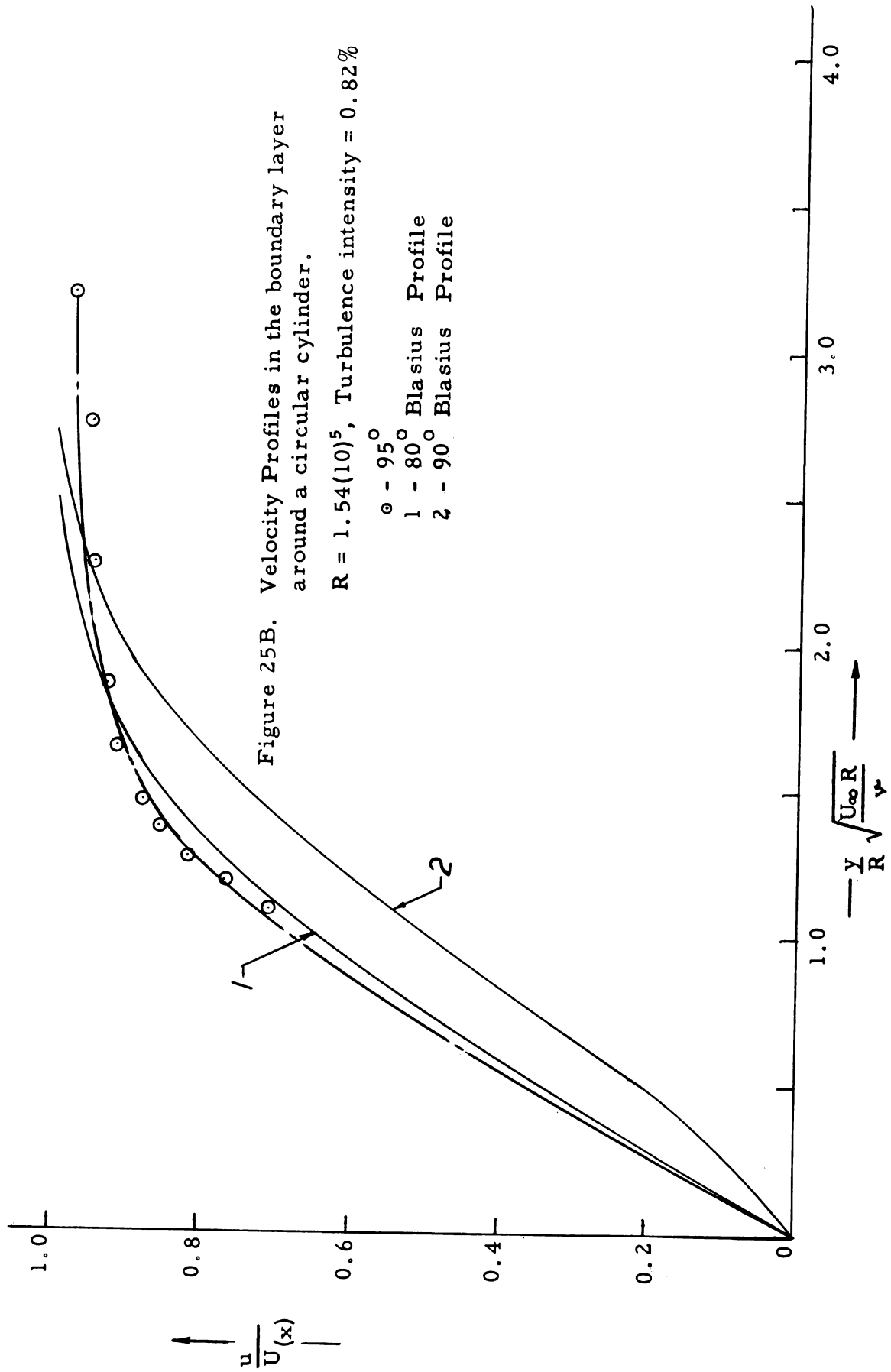
their not observing the fluctuations are the large inertia of the manometric fluid and far less sensitivity of a surface tube to velocity fluctuations as compared to that of a hot wire probe filament. In general, it is not possible to establish the transition region clearly with the help of the results presented in Figures 20 to 24. Consequently, this method was abandoned in favor of using velocity profiles in establishing the transition region.

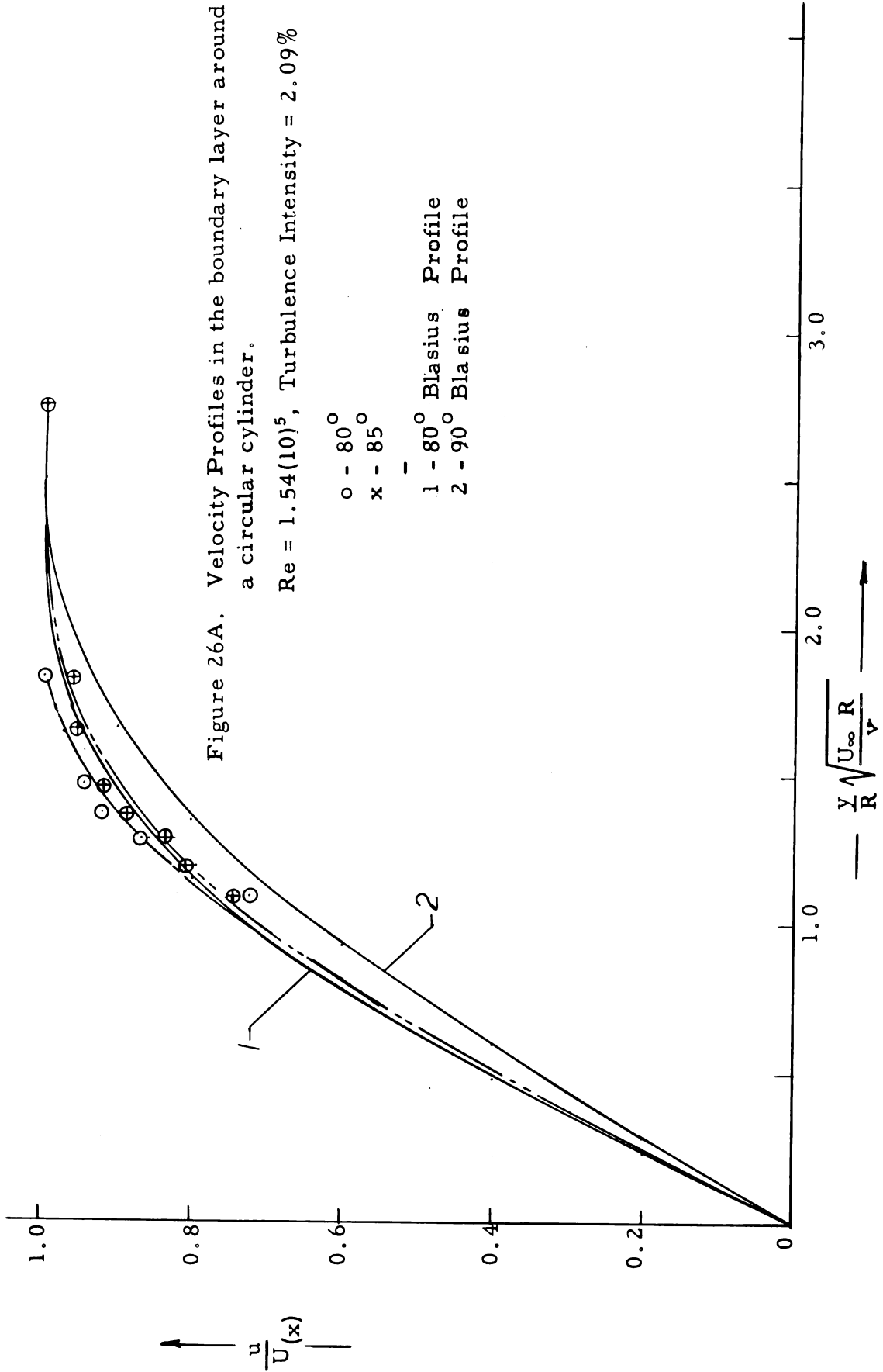
Velocity Profiles

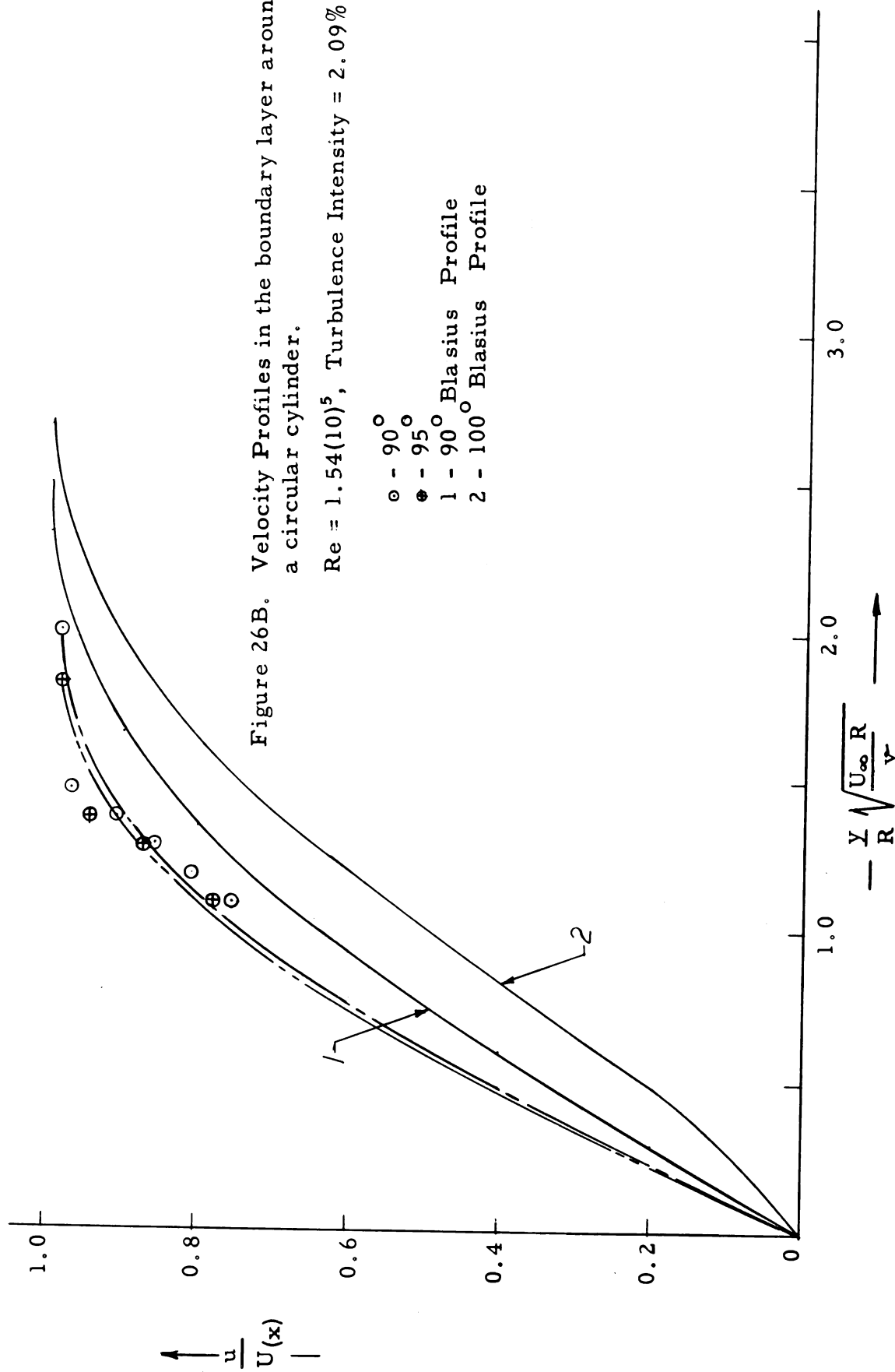
The velocity profiles, measured with a hot wire anemometer probe at various locations around the circular cylinder for various free stream turbulence intensities, are presented in Figures 25 to 28. The Blasius velocity profiles [22] for laminar boundary layer at angles of 80° , 90° and 100° from the stagnation point around a circular cylinder are also reproduced in these figures. The experimental velocity profiles for $\Theta = 85^\circ$, 90° and 95° represented in Figure 25A, B are indicative of increased steepness and boundary layer thickness as compared to the steepness and the boundary layer thickness represented by the Blasius velocity profiles for the corresponding angles. The accuracy of the precision current measuring circuit is claimed by Flow Corporation to be about 0.25 ma. These features, viz. increased steepness and boundary layer thickness, are characteristics of turbulent flow. The results of Figure 26A, B are very inconclusive in defining the transition region. The velocity profiles for $\Theta = 90^\circ$ and 95° in Figure 27A, B indicate turbulent flow at these locations, whereas, the velocity profiles for $\Theta = 100^\circ$ and 105° are steep, but do not indicate increased boundary layer thickness. In Figure 28B the velocity profiles for $\Theta = 95^\circ$ and 100° indicate turbulent flow.

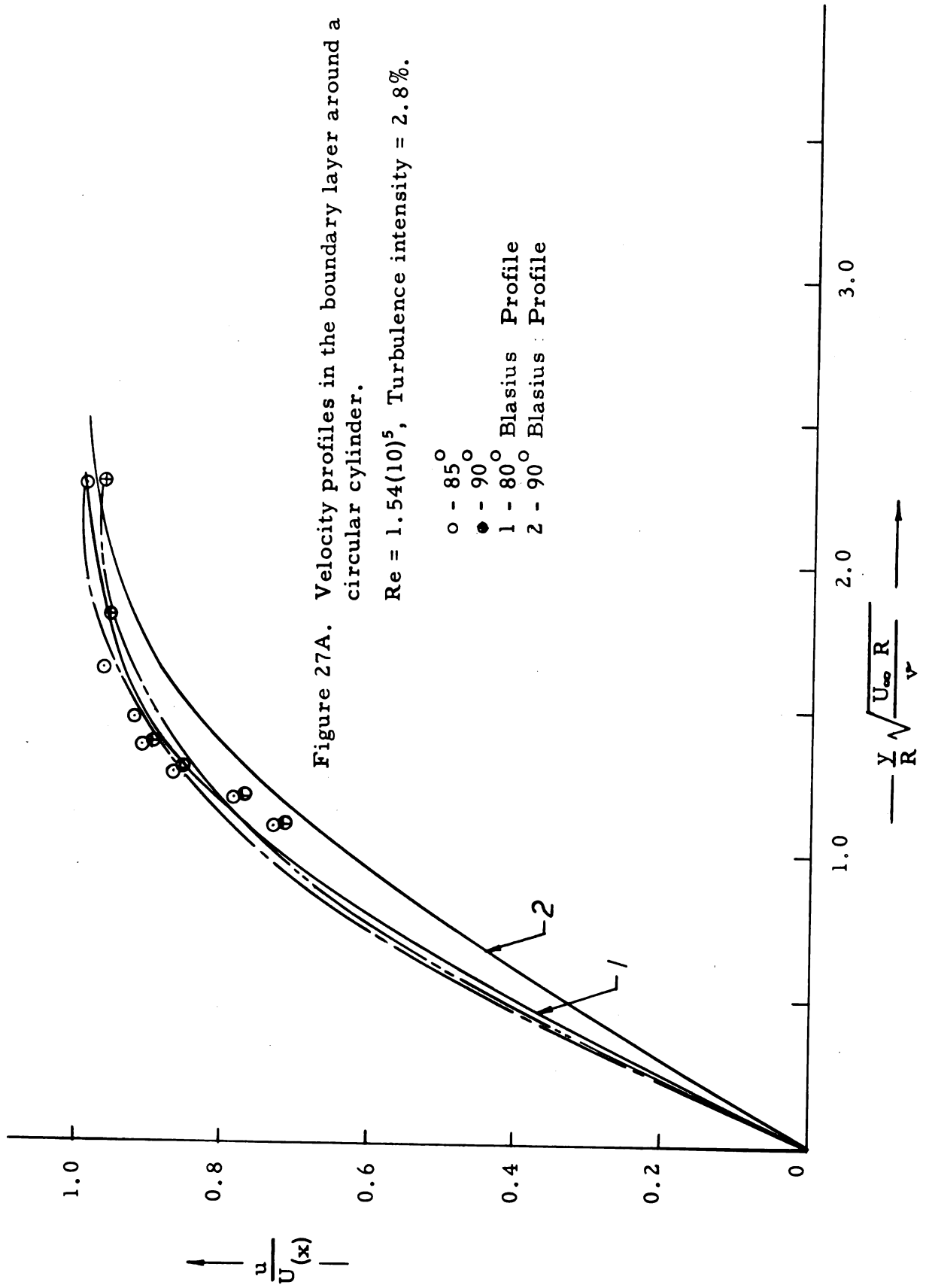
Considering the ambiguity of the results discussed above in defining the transition region clearly, and the impracticability of obtaining the velocity profiles at intervals of one degree, it was decided to give up this











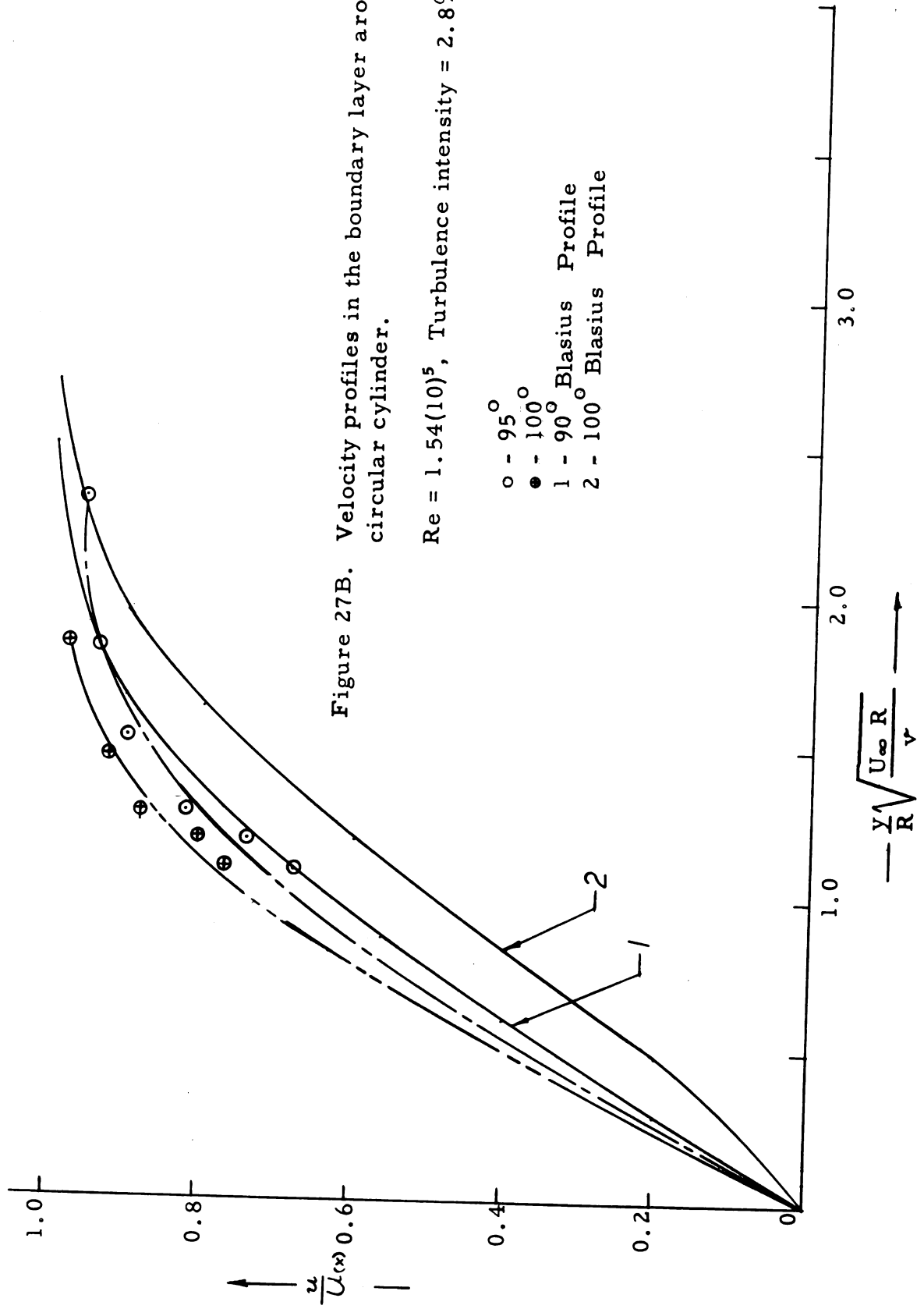


Figure 27B. Velocity profiles in the boundary layer around a circular cylinder.

Re = 1.54(10)⁵, Turbulence intensity = 2.8%

- - 95°
- - 100°
- 1 - 90° Blasius Profile
- 2 - 100° Blasius Profile

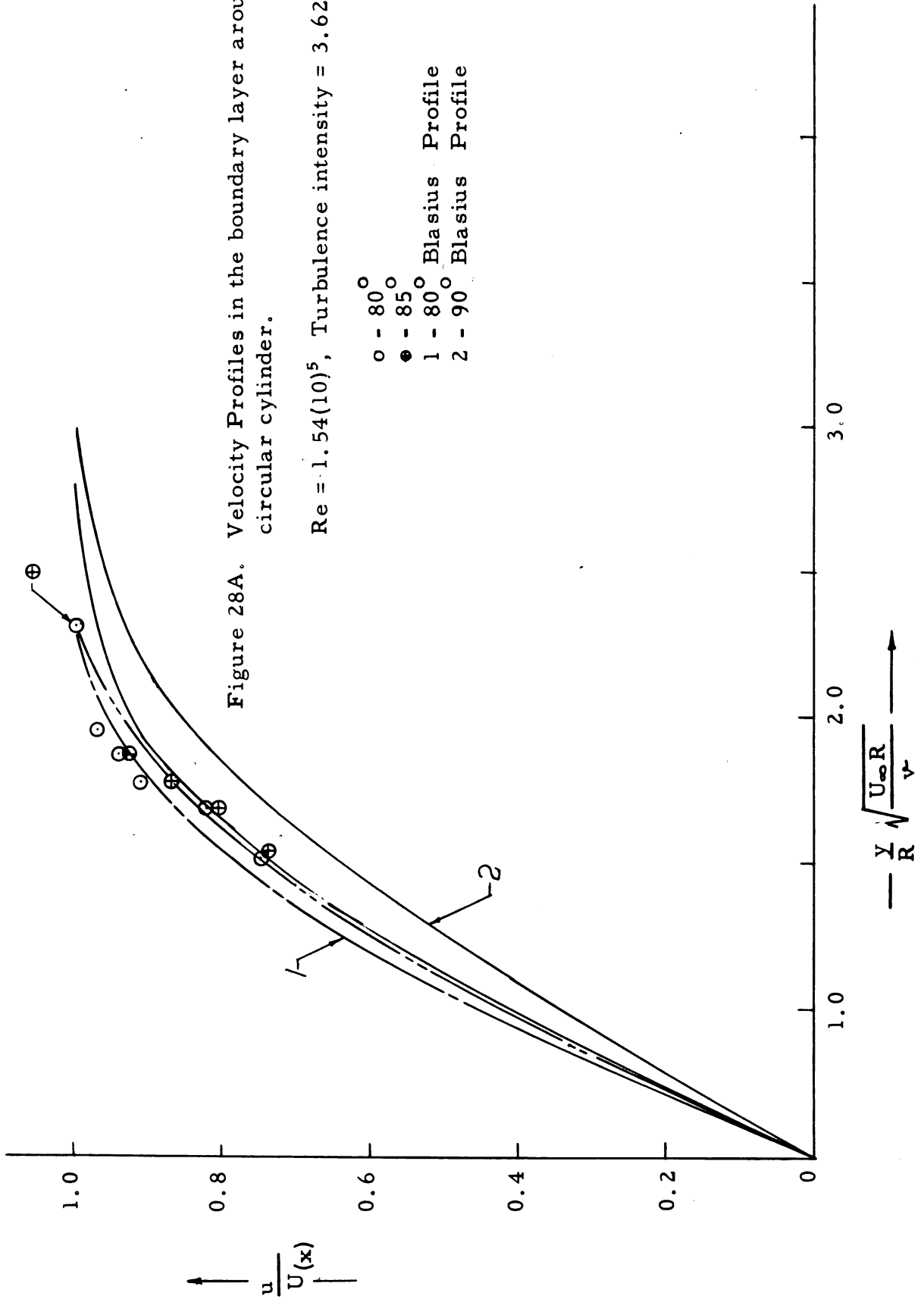
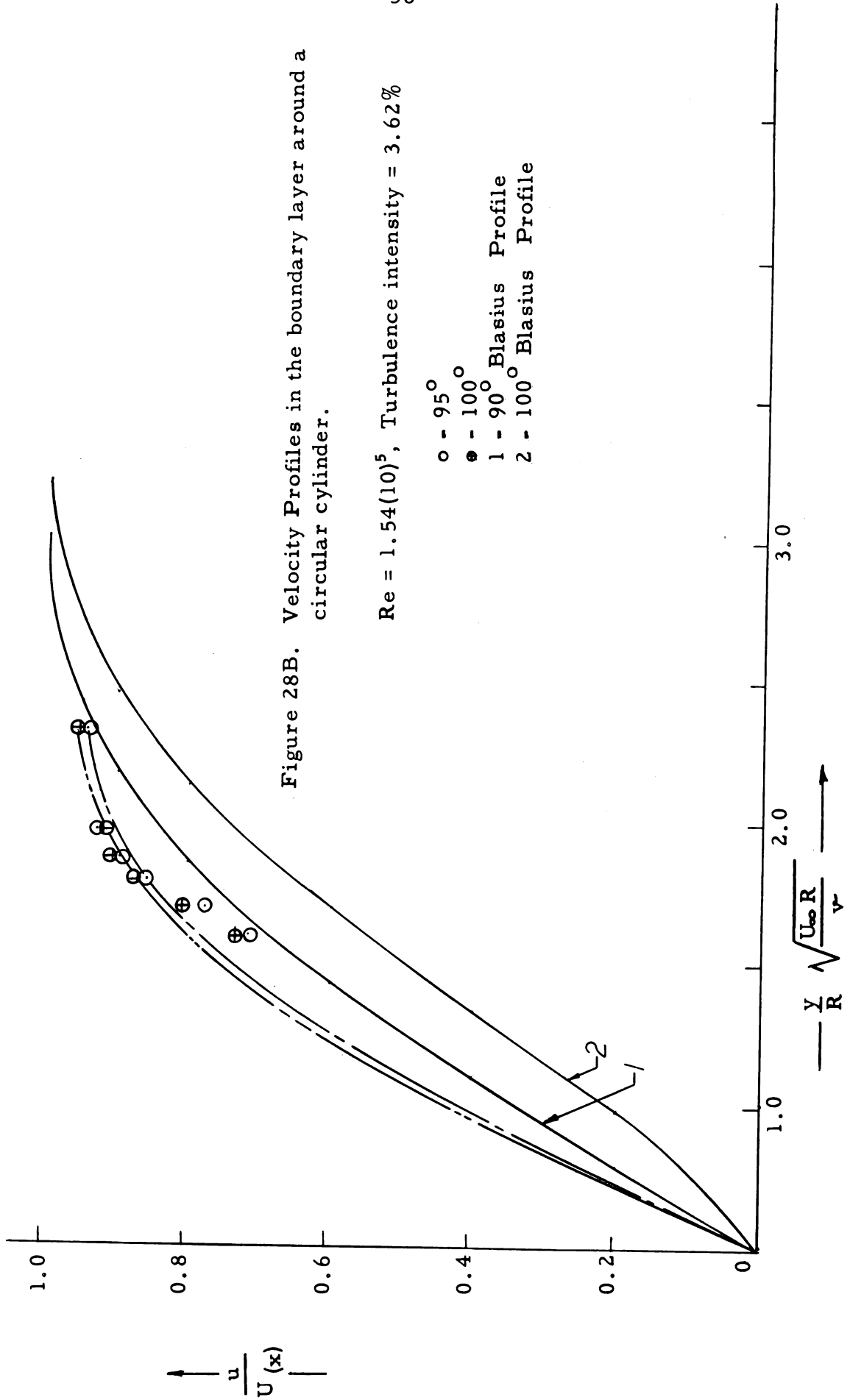


Figure 28B. Velocity Profiles in the boundary layer around a circular cylinder.

Re = 1.54(10)⁵, Turbulence intensity = 3.62%

- - 95°
- - 100°
- 1 - 90° Blasius Profile
- 2 - 100° Blasius Profile



method in establishing the transition region in favor of observing the output signal from the hot wire probe filament for the appearance of turbulent spots.

Observation of Turbulent Spots

The hot wire probe filament, which was sensitive to velocity fluctuation u , was located 0.012 inch away from the surface of the cylinder. The output signal from the hot wire anemometer amplifier was fed to a pair of Spencer-Kennedy variable electronic filters. The filters allowed the frequency band consisting of 25 Cps and 20 Kcps to pass. The output signal from the filters was led to a Tektronix cathode ray oscilloscope.

The records of the wave form of the signal fed to the cathode ray oscilloscope were made by photographing the screen of a cathode ray oscilloscope with a polaroid camera. These records are shown in the pictures of top row in Figure 31. Various conditions, e. g. turbulence intensity, angle from the stagnation point, etc., applicable to these records are also stated in Figure 31. According to Dryden [5], the frequency of fluctuations increases remarkably in the transition region. This is verified by the traces represented in the top row pictures of Figure 31. However, Schubauer [23] pointed out that it was not possible to use this increase in frequency as a criterion in establishing transition. Since then Emmons [7] and Schubauer and Klebanoff [24] have established the existence of turbulent spots, which are represented by sudden fluctuations on the screen of a cathode ray oscilloscope. These fluctuations were found to have frequencies much larger than the regular oscillations in a laminar boundary layer. Keeping these facts in mind it was realized that the records could be considerably more instructive if the low frequency variations could be eliminated. The elimination of the low frequency oscillations was very successfully achieved by using Spencer-Kennedy variable electronic filters. The filters

were used to pass the frequency band of 1 kcps-20 kcps, and extremely clear results were obtained, as shown in all the pictures of Figures 29, 30, and 31, except those 3.62% in Figure 31, for which the frequency band allowed to pass consisted of 25 cps-20 kcps. From these pictures it can be seen clearly that, in the laminar part of the boundary layer, there are regular fluctuations of low frequency representing amplified sinusoidal waves [24]. These pictures also show clearly sudden irregular fluctuations consisting of large amplitudes and high frequency. As established by Schubauer and Klebanoff [24] these large fluctuations indicate turbulent spots in the transition region. Schubauer and Klebanoff made their investigation at an extremely low level of free stream turbulence, of the order of 0.02%, however, by using electronic filters it is possible to observe turbulent spots and establish the transition region for cases involving very large free stream turbulence intensities. In the literature, the beginning of the transition region is considered as that location where a turbulent spot is first observed, and the end of the transition region as that where only turbulent spots are observed at all times.

These oscillograms also confirm some of the findings of Schubauer and Klebanoff [24], namely, the appearance of the turbulent spots for a gradually larger fraction of time as the distance from the origin of the transition region increases, and the intermittent nature of flow in the boundary layer in the transition region. As far as the author of the present investigation knows, turbulent spots have not been observed in the transition region around a circular cylinder before. Figure 32 shows the angular extent of the transition region for various free stream turbulence intensities at a Reynolds number of $1.54(10)^5$.

The results presented in Figure 32 were obtained from the oscillograms presented in Figures 29, 30 and 31. Each oscillogram represents the condition of flow in the boundary layer for one twentieth of a second at the location stated next to any oscillogram. The oscillograms were

taken in the region including the origin of the transition region roughly at intervals of four degrees to find approximately the location of the origin of the transition region. Around this approximate location of the transition zone, the oscillograms were taken at intervals of one degree to establish the origin more accurately. The origin of the transition region was regarded to be that location where the first turbulent spot was observed, and the end of the transition region as the location where only the turbulent spots were observed in the oscillogram corresponding to the location.

The present investigation was carried out for a Reynolds number of $1.54(10)^5$. The scale of free stream turbulence was not measured. However, based on the theoretical and experimental data presented in reference [2], the scale of free stream turbulence three inches ahead of the stagnation point of the cylinder for the various turbulence grids used during this investigation was as follows:

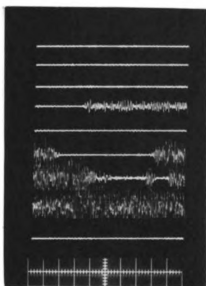
<u>Bar Size</u>	<u>Scale of Turbulence</u>
No grid	--
0.068 inch	0.095 inch
0.190 inch	0.159 inch
0.329 inch	0.217 inch
0.500 inch	0.265 inch

Under these conditions the results obtained during the present investigation demonstrate that an addition of the free stream turbulence intensity produces a rearward movement of the origin of the transition region. The different behavior on the circular cylinder presumably arises from changes in the normal pressure distribution caused by the addition of turbulence in the critical region [30]. Also, for the conditions under which the present investigation was made, the experimental results obtained here indicate that the transition region is smaller for large levels of free stream turbulence than for small turbulence intensities in the

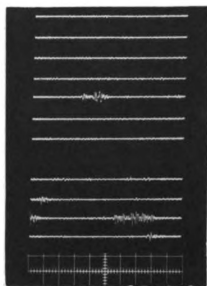
the case of a circular cylinder, as shown in Figure 32.

According to Taylor's theory, transition due to turbulence results from momentary separation of the boundary layer. It is caused by the pressure gradients within the layer resulting from the fluctuating pressure gradients of the turbulence. The separation causes the formation of a free shear layer within the boundary layer; the scale of the newly formed shear layer being an order of magnitude lower than that of boundary layer. If the Reynolds numbers of these shear layers are sufficiently high, small scale turbulence will be generated and spread through the boundary layer. The shear layer rolls up into discrete vortices of a very small scale, or turbulent spots, which diffuse through the boundary layer [31]. The present investigation confirms that transition in the boundary layer is accompanied by the formation of turbulent spots, and confirms Taylor's postulation indirectly.

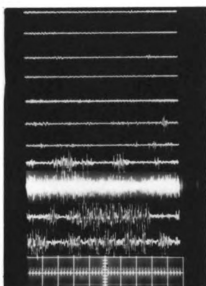
θ
in Degs.

 θ
in Degs.


Turbulence Intensity = 0.82 %



Turbulence Intensity = 0.82 %



Turbulence Intensity = 2.09 %

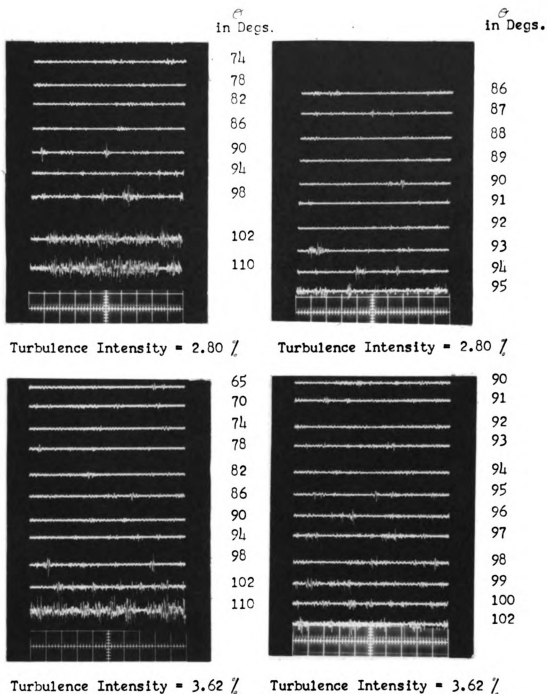


Turbulence Intensity = 2.09 %

The following conditions apply to all the pictures above:

1. Reynolds number = 1.54(10)⁵
2. Trace speed = 0.005 sec/cm.
3. Trace sensitivity = 0.5 volt/cm.
4. Location of filament from cylinder = 0.012°

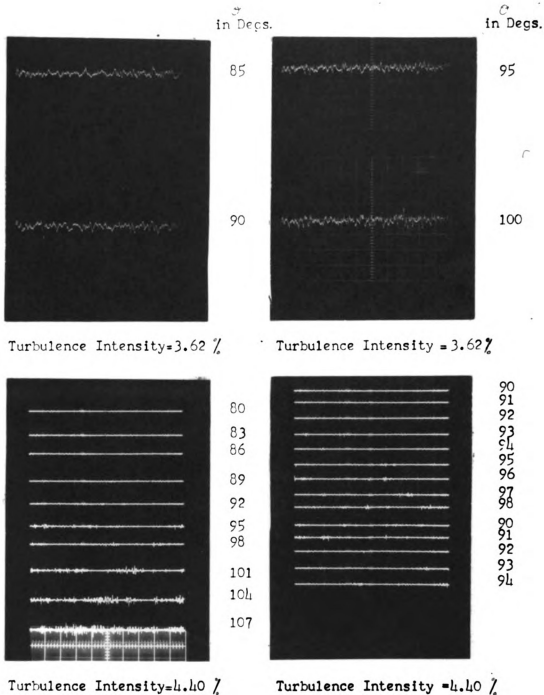
FIGURE 29. Velocity fluctuation, u , in the boundary layer around a circular cylinder.



The following conditions apply to all the pictures above:

1. Reynolds number = $1.54(10)^5$
2. Trace speed = 0.005 sec/cm.
3. Trace sensitivity = 0.5 volt/cm.
4. Location of filament from cylinder = 0.012

FIGURE 30. Velocity fluctuation, u , in the boundary layer around a circular cylinder.



The following conditions apply to all the pictures above:

1. Reynolds number = $1.54(10)^5$
2. Trace speed = 0.005 sec/cm.
3. Trace sensitivity = 0.5 volt/cm.
4. Location of filament from cylinder = 0.012"

FIGURE 31. Velocity fluctuation, u , in the boundary layer around a circular cylinder.

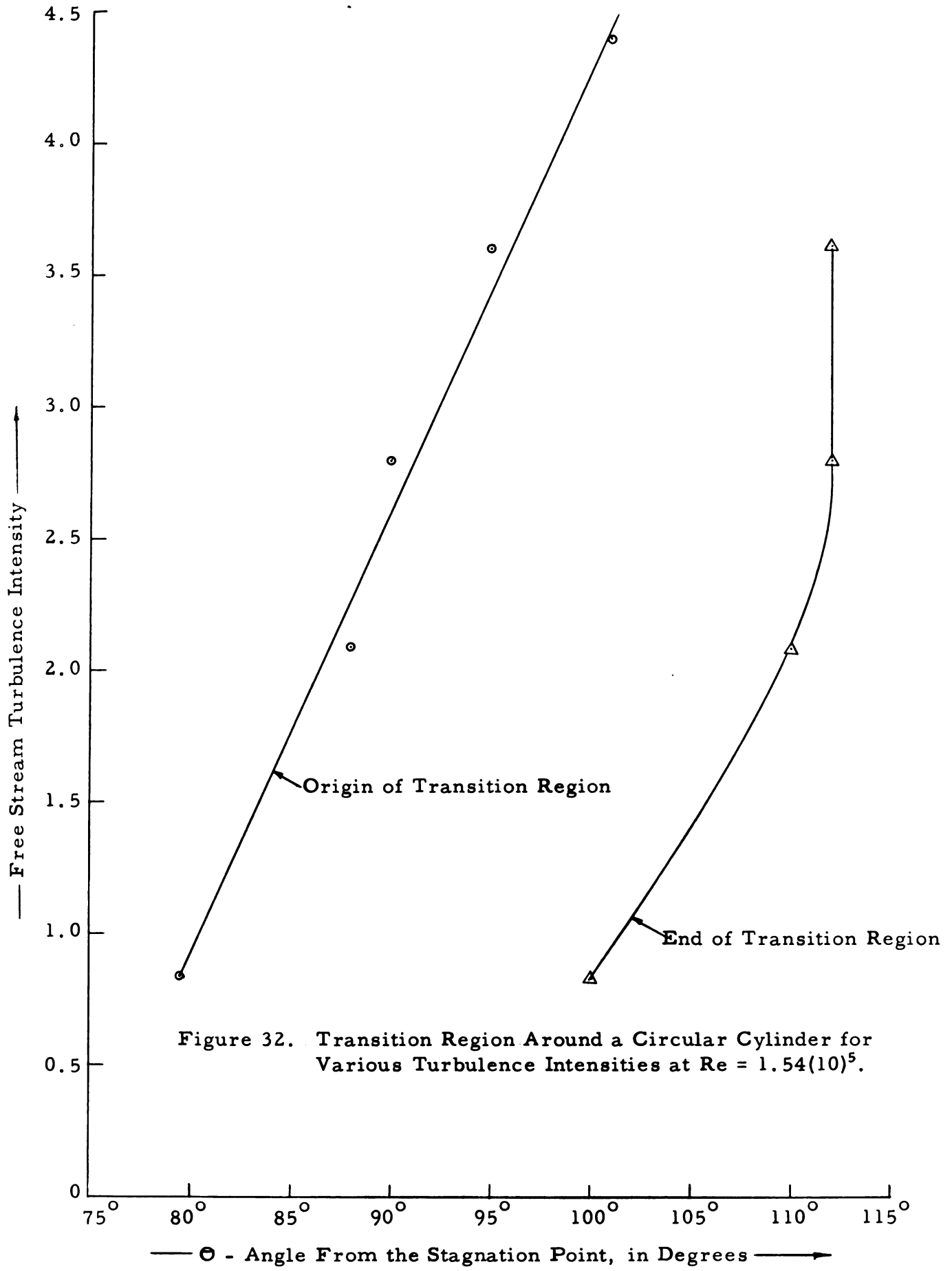


Figure 32. Transition Region Around a Circular Cylinder for Various Turbulence Intensities at $Re = 1.54(10)^5$.

CHAPTER V

CONCLUSIONS

It was observed that an increase of free stream turbulence intensity produced an increase of steepness in the velocity profiles in the outer part of the boundary layer around a circular cylinder, which means that further deviation of the velocity profiles in the outer part of the boundary layer from the Blasius profiles takes place as the free stream level of turbulence increases. The most probable reason for this phenomenon was considered to be the diffusion of turbulence in the outer region of the boundary layer.

The distributions of the coefficient of skin friction around a circular cylinder were obtained with a hot wire anemometer, as shown in Figures 20 to 24. Fage and Faulkner [8] observed a sharp minimum in the vicinity of $\Theta = 85^\circ$ after which the skin friction intensity increased till a sharp maximum was reached. After this maximum the skin friction intensity decreased gradually up to the point of separation of the boundary layer where the skin friction intensity becomes zero. Fage and Faulkner interpreted the points of minimum and maximum as the start and the end of the transition region respectively. During the present investigation a sharp minimum and a sharp maximum as described above were not observed. However, large fluctuations in these curves were observed in the transition region. These fluctuations do not represent the scattering of data because, the fluctuations were observed even when the data was taken several times. It is believed that these fluctuations were caused by the random appearance of turbulent spots. Such fluctuations were not

reported by Fage and Faulkner who used surface tubes in their investigation. The probable reasons for their not being able to observe these fluctuations are the inertia of the manometric fluid and markedly less sensitivity of a surface tube to fluctuations as compared to a hot wire probe filament. This method was found to be incapable of establishing the transition region accurately.

The velocity profiles at various stations around a circular cylinder were obtained with a hot wire anemometer for various conditions, as shown in Figures 25 to 28. As explained in Chapter IV, page 48, a part of the results were quite conclusive in establishing transition, while the rest proved unsuccessful. Due to the incapability of these results in establishing the transition region and the impracticability of measuring velocity profiles at intervals of one degree this method was given up.

Records of the wave form of the output signal from the filament of a hot wire probe were made from the screen of a cathode ray oscilloscope with a polaroid camera, as shown in Figures 29 to 31. This method proved highly successful in defining the transition region. The existence of turbulent spots, and the intermittent nature of the flow in the boundary layer were clearly observed in the transition region of the boundary layer around the circular cylinder. These characteristics of the boundary layer on a flat plate were reported in reference [24], however, it is believed that for the case of a circular cylinder they have not been reported before.

It was found that contrary to the case of a flat plate, an increase in the free stream turbulence intensity produces a rearward movement of the origin of the transition, as shown in Figure 32. Also, it was observed that the transition region became smaller with a marked increase in the free stream turbulence intensity. For the limitations of these results refer to pages 58, 58a and 58b. A possible explanation for the surprising effect of free stream turbulence intensity on the origin of the transition region in the boundary layer around a circular cylinder as compared to that of a flat plate and airfoils is also presented on page 58a.

SUGGESTED PROBLEMS

The new problems encountered during the present investigation that need further study are summarized below:

(1) In the case of a flat plate an increase in the free stream turbulence intensity has been observed to produce a forward movement, i. e. towards the leading edge, of the point of origin of the transition region. However, in the case of a circular cylinder, the point of origin of the transition region moves further away from the stagnation point when the free stream turbulence intensity is increased. It is important to determine the critical static pressure distribution for which the reverse trend in the movement of the point of origin of the transition region results. Various pressure distributions can be obtained by using elliptic cylinders of various ratios of the major to the minor axis.

(2) It is known that the appearance of turbulent spots is a statistical phenomenon, and the transition from laminar to turbulent flow in the boundary layer is closely connected to intermittency factor, which represents fraction of the time a point spends in turbulent flow. In literature the intermittency factor has been obtained so far by photographing the screen of a cathode ray oscilloscope with a movie camera. This method of determining intermittency factor involves large amounts of film, and time in scanning the film. Also, due to the statistical nature of the phenomena this method of determining intermittency factor does not necessarily guarantee accuracy. A better method which needs further study is to use electronic instruments which would record the turbulent spots and other useful information about them.

(3) The effect of pressure distribution on the intermittency factor has not been reported in the literature so far, and needs to be investigated.

(4) Another problem that needs investigation is the distribution of the intermittency factor across the boundary layer.

(5) The mechanics of spot creation and growth is as yet not completely clear, and needs further investigation.

BIBLIOGRAPHY

1. Adelberg, M., Ph. D. Dissertation, Purdue University, 1957.
2. Bains, W. D. and Patterson, E. G., An Investigation of Flow Through Screens, Trans. Amer. Soc. Mech. Engrs. 73, 467 (1951).
3. Dhawan, S., Direct Measurements of Skin Friction, NACA Tech. Note 2567, 1952.
4. van Driest, E. R. and J. E. Boison, Experiments on Boundary Layer Transition at Supersonic Speeds. J. Aero. Sci., Vol. 24, No. 12, 1957.
5. Dryden, H. L., Air Flow in the Boundary Layer Near a Plate, NACA, Tech. Rept. 562, 1936.
6. Dryden, H. L., Review of Published Data on the Effect of Roughness on Transition from Laminar to Turbulent Flow. Jour. Aero. Sci. 20, 477-482, 1953.
7. Emmons, H. W., The Laminar Turbulent Transition in a Boundary Layer, Jour. Aero. Sci. 19, No. 1, 1952; Part II ASME 859-868, 1952.
8. Fage, A. and Faulkner, F. M., Further experiments on the Flow Around a Cylinder, R&M No. 1369, Great Britain Aeronautical Research Committee, 1931.
9. Flow Corp'n. Bulletin No. 37B, "Model HWB2 Hot Wire Anemometer Theory and Instruction."
10. Flow Corporation Bulletin No. 16, "Instructions for Using Model HW1 Hot Wire Sum Difference Control Unit."
11. Froude, W., Experiments on the Surface Friction. British Assn. Rept. 1872.
12. Giedt, W. H., Effect of Turbulence Level of Incident Air Stream on Local Heat Transfer and Skin Friction on a Cylinder, Jour. Aero. Sci. No. 1951.

13. Hinze, J. O., An Introduction to the Theory and Mechanism of Turbulence, McGraw-Hill Book Co., Inc., New York, 1959.
14. von Karman, Theodore, The Analogy Between Fluid Friction and Heat Transfer, Trans. ASME., Vol. 61, No. 8, Nov. 1939.
15. King, L. V., Phil Trans. Roy. Soc. London, 214A, 373 (1914).
16. Kramers, H., Physica, 12, 61 (1946).
17. Kuethe, A. M. and Schetzer, J. D., Foundations of Aerodynamics, John Wiley and Sons, Inc., New York, 1959.
18. Liepmann, H. W. and Dhawan, S., Proc. 1st U. S. Nat. Cong. Applied Mech., 1951.
19. Lin, C. C., Hydrodynamical Stability, Cambridge University Press, Cambridge, 1955.
20. Pankhurst and D. W. Holder, Wind Tunnel Technique, Pitman and Sons, London, 1952.
21. Reynolds, O., Trans. Roy Soc. London, 174A, 935 (1882).
22. Schlichting, H. Boundary Layer Theory, McGraw-Hill Book Co., Inc., New York, 1960.
23. Schubauer, G. B., Air Flow in the Boundary Layer of an Elliptic Cylinder, NACA, Tech. Rept. No. 652, 1939.
24. Schubauer, G. B. and Klebanoff, P. S., Contributions on the Mechanics of Boundary Layer Transition, NACA Tech. Note 3489, 1955.
25. Schubauer, G. B. and Skramstad, H. R., Laminar Boundary Layer Oscillations and Stability of Laminar Flow, Jour. Aero. Sci., Vol. 14, 69, 1947; NACA W-B Rept. 909, 1947.
26. Schultz, Grunow, F. NACA TM No. 986, 1941 (Translation).
27. Taylor, G. I., Proc. Roy Soc. London, A156, 307 (1936).

28. Wills, J. A. B., The Correction of hot-wire readings for proximity to a solid boundary, *Journal of Fluid Mechs.* Vol. 12, 388-396, March 1962.
29. Zahm, A. F., Flow and Drag Formulas for Simple Quadratics NACA Tech. Rept. 253, NACA, 1927.
30. Goldstein, S., Modern Developments in Fluid Dynamics, Vol. 2, p. 426, Oxford, 1957.
31. Lin, C. C., Turbulent Flows and Heat Transfer, Princeton University Press, 1959.

ROOM USE ONLY

1. [Illegible]

